Drivers of Holocene sea–level change in the Caribbean

Article *in* Quaternary Science Reviews · January 2017

DOI: 10.1016/j.quascirev.2016.08.032

11 authors, including:

Nicole S. Khan
United States Geological Survey
24 PUBLICATIONS **131** CITATIONS
SEE PROFILE

A. Dutton
University of Florida
57 PUBLICATIONS **1,324** CITATIONS
SEE PROFILE

Robert E. Kopp
Rutgers, The State University of New Jersey
130 PUBLICATIONS **3,190** CITATIONS
SEE PROFILE

Christopher H Vane
British Geological Survey
103 PUBLICATIONS **1,754** CITATIONS
SEE PROFILE

Quaternary Science Reviews 155 (2017) 13–36

Contents lists available at ScienceDirect

Quaternary Science Reviews

journal homepage: www.elsevier.com/locate/quascirev

Invited review

Drivers of Holocene sea-level change in the Caribbean

Nicole S. Khan [a, b, c, *], Erica Ashe [b, c, d, e], Benjamin P. Horton [b, c, f], Andrea Dutton [g], Robert E. Kopp [h, c], Gilles Brocard [i], Simon E. Engelhart [j], David F. Hill [k], W.R. Peltier [l], Christopher H. Vane [m], Fred N. Scatena [i]

[a] U.S. Geological Survey, St Petersburg Coastal and Marine Science Center, St Petersburg, FL 33701, USA
[b] Sea Level Research, Department of Marine and Coastal Sciences, Rutgers University, New Brunswick, NJ, 08091, USA
[c] Institute of Earth, Ocean & Atmospheric Sciences, New Brunswick, NJ, 08901, USA
[d] Department of Statistics and Biostatistics, Rutgers University, Piscataway, NJ, 08854, USA
[e] CCICADA (Command, Control, and Interoperability Center for Advanced Data Analysis, A Department of Homeland Security Center of Excellence), USA
[f] Earth Observatory of Singapore, Asian School of the Environment, Nanyang Technological University, Singapore
[g] Department of Geological Sciences, University of Florida, Gainesville, FL, 32611, USA
[h] Department of Earth & Planetary Sciences and Rutgers Energy Institute, Rutgers University, Piscataway, NJ, 08854, USA
[i] Department of Earth and Environmental Science, University of Pennsylvania, 240 S 33rd St., Philadelphia, PA, 19104, USA
[j] Department of Geosciences, University of Rhode Island, Kingston, RI, 02881, USA
[k] Department of Civil and Construction Engineering, Oregon State University, Corvallis, OR, 97331, USA
[l] Department of Physics, University of Toronto, Toronto, Canada
[m] British Geological Survey, Environmental Science Centre, Keyworth, Nottingham, NG12 5GG, UK

ARTICLE INFO

Article history:
Received 22 May 2016
Received in revised form
25 August 2016
Accepted 26 August 2016

Keywords:
Holocene
Relative sea level
Caribbean
Glacial-isostatic adjustment
Vertical tectonic motion
Hierarchical statistical modeling

ABSTRACT

We present a Holocene relative sea-level (RSL) database for the Caribbean region (5°N to 25°N and 55°W to 90°W) that consists of 499 sea-level index points and 238 limiting dates. The database was compiled from multiple sea-level indicators (mangrove peat, microbial mats, beach rock and acroporid and massive corals). We subdivided the database into 20 regions to investigate the influence of tectonics and glacial isostatic adjustment on RSL. We account for the local-scale processes of sediment compaction and tidal range change using the stratigraphic position (overburden thickness) of index points and paleotidal modeling, respectively. We use a spatio-temporal empirical hierarchical model to estimate RSL position and its rates of change in the Caribbean over 1-ka time slices. Because of meltwater input, the rates of RSL change were highest during the early Holocene, with a maximum of 10.9 ± 0.6 m/ka in Suriname and Guyana and minimum of 7.4 ± 0.7 m/ka in south Florida from 12 to 8 ka. Following complete deglaciation of the Laurentide Ice Sheet (LIS) by ~7 ka, mid-to late-Holocene rates slowed to < 2.4 ± 0.4 m/ka. The hierarchical model constrains the spatial extent of the mid-Holocene highstand. RSL did not exceed the present height during the Holocene, except on the northern coast of South America, where in Suriname and Guyana, RSL attained a height higher than present by 6.6 ka (82% probability). The highstand reached a maximum elevation of +1.0 ± 1.1 m between 5.3 and 5.2 ka. Regions with a highstand were located furthest away from the former LIS, where the effects from ocean syphoning and hydro-isostasy outweigh the influence of subsidence from forebulge collapse.

1. Introduction

Changes in relative sea level (RSL, the height of the ocean surface relative to the land surface or ocean floor) in the Caribbean during the Holocene are driven by eustatic, glacial isostatic adjustment (GIA), tectonic and local factors that act over a variety of spatial and temporal scales (Peltier, 1998; Milne et al., 2009).

Eustatic sea-level (ESL) change (i.e., sea-level equivalent or ocean volume change) in the Holocene is dominated by Northern Hemisphere deglaciation (Lambeck et al., 2014), with varying rates of RSL rise suggested from GIA modeling. At the start of the Holocene ~11.7 ka, ESL was ~60 m below present and rose at rate of ~15 m/ka from ~11.4 to 8.2 ka (Lambeck et al., 2014). The rate of ESL

* Corresponding author. U.S. Geological Survey, St Petersburg Coastal and Marine Science Center, St Petersburg, FL 33701, USA.
E-mail address: nkhan@usgs.gov (N.S. Khan).

http://dx.doi.org/10.1016/j.quascirev.2016.08.032
0277-3791/

rise decreased from ~8 to 7 ka, consistent with the final phase of Laurentide Ice Sheet (LIS) deglaciation at ~7 ka, followed by a progressive decrease in the rate of rise from 7 ka to present (Peltier, 2004; Lambeck et al., 2014; Peltier et al., 2015; Bradley et al., 2016).

As the rate of ESL rise decreased in the Holocene, processes associated with GIA dominated the temporal and spatial pattern of RSL change (Milne et al., 2005; Milne and Peros, 2013). The magnitude of subsidence associated with the collapsing LIS forebulge diminishes with distance from the regions of peak forebulge collapse near the former LIS margin; therefore, in the Caribbean, located >2000 km away from the LIS margin, the magnitude of this signal lessens and signals from ocean syphoning, hydro-isostatic loading and perturbations to Earth's rotation vector become dominant and may create a higher than present RSL, i.e., a mid-Holocene highstand (Peltier et al., 1978; Pirazzoli, 1991; Mitrovica and Peltier, 1991; Peltier, 1998; Milne and Mitrovica, 1998; Mitrovica and Milne, 2002; Milne et al., 2005). However, the spatial extent of forebulge subsidence and emergence of mid-Holocene highstands on Caribbean continental margins is not well documented, in part because of its active tectonic setting.

The complex tectonic setting of the Caribbean region also influences RSL. The Caribbean plate interacts with the North American, South American, Nazca and Cocos plates, each characterized by a diversity of tectonic regimes (Benz et al., 2010). Inclined zones of deep earthquakes (Wadati-Benioff zones), deep ocean trenches, and volcanic arcs indicate subduction of oceanic lithosphere along the Central American and Atlantic Ocean margins of the Caribbean plate (Dixon et al., 1998; DeMets et al., 2000; Benz et al., 2010). Shallow seismicity and focal mechanisms of major shocks in Guatemala, northern Venezuela and the Cayman Ridge/Trench indicate transform fault and pull-apart basin tectonics (Weber et al., 2001; Benz et al., 2010). Furthermore, lateral variations in mantle viscoelastic structure from a high-viscosity slab associated with subduction of the South American Plate beneath the Caribbean Plate have been shown to suppress local GIA deformation and decrease RSL rise predicted during deglaciation (Austermann et al., 2013). The combined effect of tectonic processes on regional Holocene RSL histories in the Caribbean, however, is unknown.

Local factors, such as changes in tidal range and sediment consolidation, affect RSL records. Temporal variations in tides occur on a global scale because of glaciation-driven changes in the availability of dissipation sites of tidal energy (e.g., Uehara et al., 2006; Griffiths and Peltier, 2008, 2009; Hill et al., 2011). These changes influence RSL reconstructions because no sea-level indicators form precisely at mean sea level (Horton et al., 2013). Sediment consolidation due to compaction of pre-Holocene strata (e.g., Horton and Shennan, 2009) and the accumulation of overlying Holocene material and land drainage (e.g., Kaye and Barghoorn, 1964; Törnqvist et al., 2008) also cause RSL reconstructions to deviate from true values.

Here, we compile a Caribbean sea-level database to provide a framework for developing our understanding of the primary mechanisms of RSL change during the Holocene. The database consists of 737 sea-level index points and limiting dates that span the period from 12 ka to present (Fig. 1). We define the indicative meanings and ages of multiple sea-level indicators including mangrove peat, microbial mats, beach rock, and corals. We account for local effects by using the stratigraphic position (overburden thickness) of index points to adjust samples for sediment compaction where appropriate (Shennan et al., 2000b; Törnqvist et al., 2008; Horton and Shennan, 2009) and provide an additional error for changes in tidal range over the Holocene using a paleotidal model (Hill et al., 2011; Hall et al., 2013; Horton et al., 2013). We consider the influence of GIA and tectonics on local RSL histories and employ a spatio-temporal statistical model to examine patterns and rates of RSL change (and their associated uncertainty) and constrain the magnitude and spatial extent of the mid-Holocene highstand in the Caribbean.

2. Methodology to reconstruct relative sea level

The standardized methodology developed by the International Geological Correlation Projects (IGCP) 61, 200, 495 and 588 (e.g., Preuss, 1979; van de Plassche, 1982; Gehrels and Long, 2007; Hijma et al., 2015) was followed to determine RSL, age, and associated errors of sea-level index points. To calculate past RSL, each sample's indicative meaning (Shennan, 1986; van de Plassche, 1986; Horton et al., 2000) must be known. The sample ages within the database were measured using ^{14}C and U–Th dating. The ^{14}C data were calibrated to years before present (where present is 1950 AD) using the most recent IntCal13 and Marine13 calibration curves (Reimer, 2013).

2.1. Indicative meaning of sea-level indicators

The indicative meaning is defined as the relationship of an indicator to sea level (van de Plassche, 1986) and has two components: the reference water level, which defines the relationship of the indicator to a contemporaneous tide level (e.g., mean higher high water [MHHW]) and the indicative range, which is the elevational range occupied by the sea-level indicator (Fig. 2). When litho-, bio-, or chemostratigraphic data indicate deposition in terrestrial or marine environments, these data provide an upper or lower limit on the position of RSL respectively and are classified as limiting dates (Shennan and Horton, 2002).

2.1.1. Mangrove and sedimentary indicators

Mangrove peats comprise most (n = 313) of the index points in the database. The vertical distribution and characteristics of mangrove species (e.g., *Rhizophora mangle, Avicennia germinans* and *Laguncularia racemosa*) are related to the frequency and duration of tidal inundation (Tomlinson, 1986; Smith, 1992; Mendelssohn and McKee, 2000). In the Caribbean, growth of peat-forming mangroves is constrained to the upper half of the intertidal zone (e.g., Davis, 1940; Thom, 1967; Twilley et al., 1996; Dawes, 1998; Davis and Fitzgerald, 2003; Lara and Cohen, 2006). Therefore, we define the indicative meaning of mangrove peat to be mean tide level (MTL) to highest astronomical tide (HAT) (Table 1). We use microfossils (e.g., Ramcharan and McAndrews, 2006; Jessen et al., 2008), $\delta^{13}C$ values (e.g., Klosowska, 2003; McKee et al., 2007) and plant macrofossils (e.g., Wooller et al., 2003; Monacci et al., 2009) to support the accumulation of peat in a mangrove environment.

Microbial mats from hypersaline lagoons comprise a small (n = 5) portion of index points in the database (Knowles, 2008). Microbial mats are predominantly formed from cyanobacteria living on bedding surfaces that aggrade vertically by cellular growth and by binding detrital particles (Gerdes and Krumbein, 1994; Gerdes, 2010). Following Livsey and Simms (2013), who surveyed the elevation of modern microbial mats from the Gulf of Mexico, we assign an indicative meaning of mean lower low water (MLLW) to MHHW.

A small number of index points (n = 5) were obtained from organic muds and peats from floodplain facies of the Orinoco Delta (Warne et al., 2002). Studies in the Mississippi River and Rhine-Meuse deltas suggest deposition between mean sea level (MSL) and mean high water (MHW) (van Dijk et al., 1991; van de Plassche, 1995; Cohen, 2003; Törnqvist et al., 2004). We take a conservative approach and assign these samples an indicative meaning of MTL to HAT.

Terrestrial limiting dates (n = 35) were derived from: (1) peat

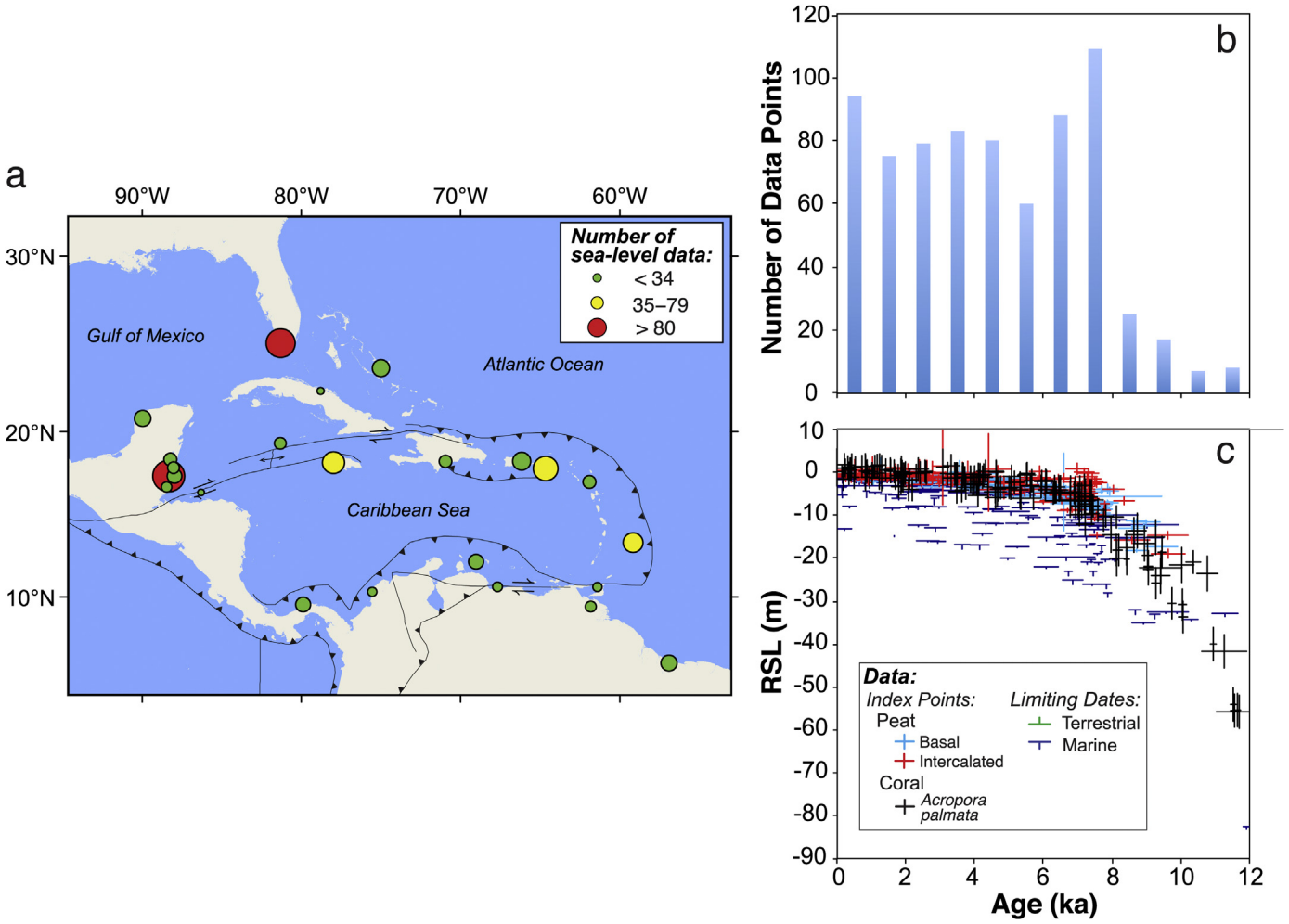

Fig. 1. Spatial and temporal distribution of Caribbean sea-level data. (a) Spatial distribution of data in the Caribbean, divided into 20 regions based on proximity to the former Laurentide Ice Sheet and local to regional tectonic setting. (b) Temporal distribution of Caribbean sea-level data. (c) Caribbean sea-level data for all 20 regions plotted by type and indicator.

containing freshwater macrofossils (e.g., Digerfeldt and Hendry, 1987) or with a stable carbon isotope signature in the range of freshwater swamp environments (e.g., $\delta^{13}C < -28$; e.g., Khan, 2014) and absent of marine indicators; (2) calcitic muds (e.g., Scholl, 1964; Scholl and Stuiver, 1967); and (3) soilstone crusts (e.g., Robbin, 1984; Gischler, 2003) formed directly above Pleistocene limestone bedrock. Terrestrial limiting dates usually form in a depositional environment above HAT, although they can form within the intertidal zone due to rising groundwater tables (e.g., Jelgersma, 1961). Therefore, a conservative lower limit of MTL is used (e.g., Shennan and Horton, 2002).

In addition to "deep-water corals" (see section 2.1.2), marine limiting dates (n = 204 total) were obtained from muds containing marine foraminifera (e.g., Cheng et al., 2012), diatoms (e.g., Velez et al., 2014), macroalgae (e.g., *Halimeda*; Macintyre et al., 2004), and *in-situ* mollusks (e.g., Klosowska, 2003). Marine limiting dates are interpreted as forming below MTL (e.g., Engelhart and Horton, 2012).

2.1.2. Coral indicators

Reef framework dominated by *Acropora palmata* (n = 172), which is characteristic of shallow-water reef crest environments in the Caribbean, was classified as an index point assumed to have formed between 0 and 5 m below MLLW (Goreau, 1959; Adey and Burke, 1976; Gladfelter et al., 1978; Lighty et al., 1982; Fairbanks, 1989; Toscano and Macintyre, 2003; Lambeck et al., 2014). We altered this indicative meaning if modern surveys were performed to examine the local depth distribution of *A. palmata* and/or shallow reef facies. For example, in Campeche, Mexico, Blanchon and Perry (2004) documented the texture, coral composition and taphonomic signatures from variations in encrustation, bioerosion and cementation in reef-front (2–10 m below MTL), reef crest-flat (0–2 m below MTL) and rubble-cay (0–5 m above MTL) zones.

Acropora cervicornis, *Colpophyllia natans*, *Diploria clivosa*, *D. labrynthiformis*, *D. strigosa*, *Dichocoenia stokesii*, *Orbicella* species complex (including *O. annularis*, *O. faveolata*, and *O. franksi*), *Porites astreoides*, and *Siderastrea siderea* all have broad depth distributions (~0–30 m; OBIS, 2016) and are hereafter referred to as "deep-water corals". We classify all deep-water corals, and *A. palmata* growing in association with these deep-water corals, as marine limiting dates with a RWL of ≤ MTL (n = 105)

2.1.3. Beach-rock indicators

A small (n = 4) number of index points from Venezuela were obtained from beach-rock indicators (Schubert et al., 1977; Valastro et al., 1977). Beach rock results from the lithification of

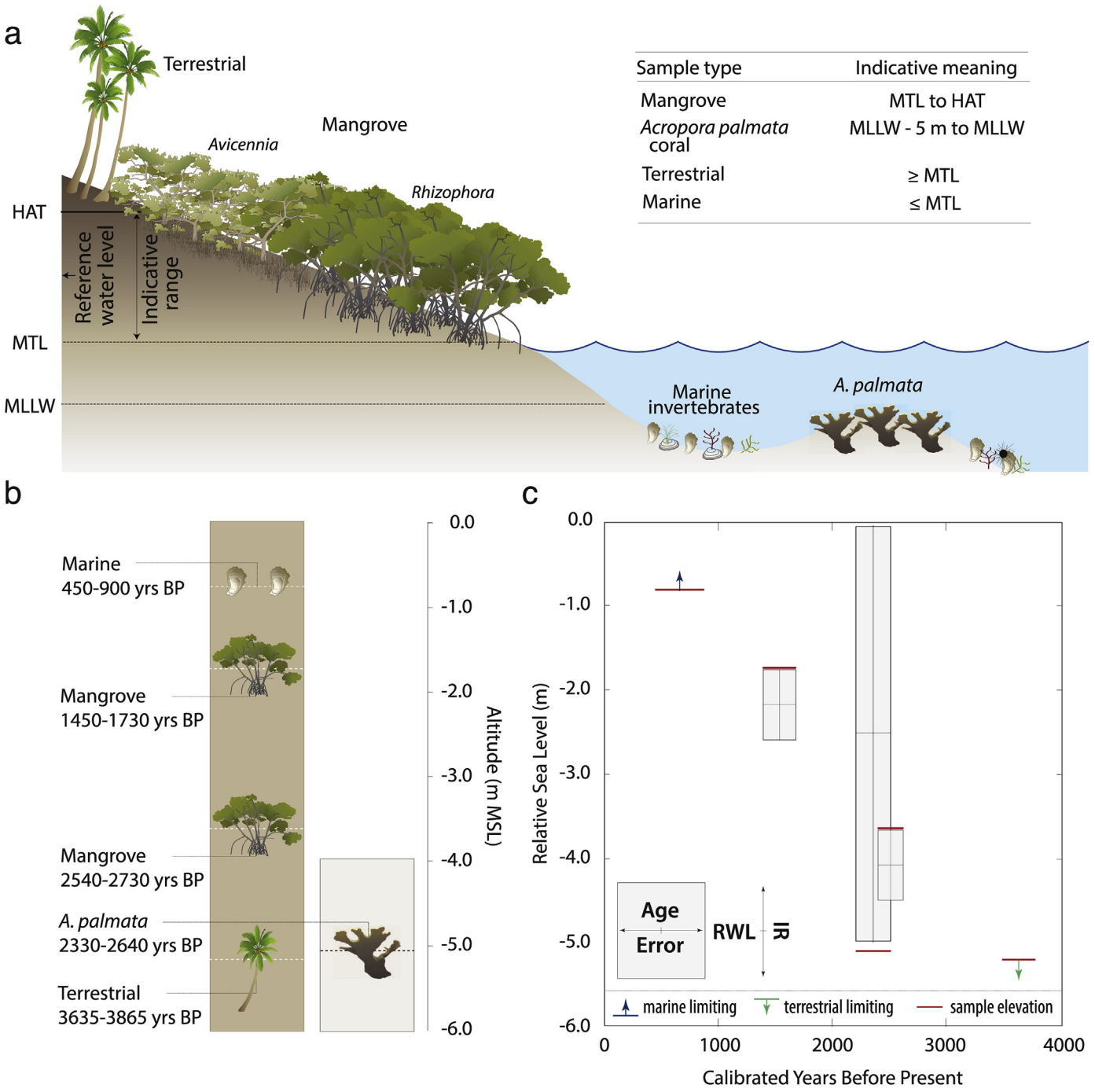

Fig. 2. Schematic representation of the indicative meaning and a theoretical example of its application to reconstruct RSL from radiocarbon-dated mangrove sediment and reef-crest cores. (a) Vertical distribution of mangrove and coral zones with respect to the tidal frame for the Caribbean region. (b) Altitude of dated samples in theoretical cores. (c) Production of sea-level index points and limiting dates. RSL is reconstructed by subtracting a sample's RWL from its altitude in a core. RWL = reference water level; IR = indicative range. RSL = relative sea level; MLLW = mean lower low water; MTL = mean tide level; HAT = highest astronomical tide. Symbols courtesy of the Integration and Application Network (ian.umces.edu/symbols/), University of Maryland Center for Environmental Science.

unconsolidated sediments by calcium carbonate cements in the intertidal zone of tropical and subtropical beaches (McLean, 2011). Dated aragonitic cements (examined in thin section, presumed to not be recrystallized calcite material) and shells formed *in situ* in the beach rock matrix were considered valid index points (Mauz et al., 2015). Following observations of the vertical distribution of beach rock by Kelsey (2015) and Mauz et al. (2015), we assign a conservative indicative meaning of MLLW to HAT to these samples.

2.2. Ages of sea-level indicators

2.2.1. Radiocarbon age calibration

The database contains radiocarbon ages that were measured by Accelerator Mass Spectrometry (AMS), Gas Proportional Counting (GPC) and Liquid Scintillation Counting (LSC) radiocarbon measurements. Approximately half (n = 287) of the samples in the database come from bulk sediment or peat samples that may have

Table 1
Criteria used to assess the indicative meaning of each sample in the Caribbean database.

Sample type	Evidence	Reference water level	Indicative range
Mangrove peat	- Mangrove plant macrofossils (e.g., Robbin, 1984) - Foraminiferal, diatom, or pollen assemblages dominated by mangrove taxa (Jessen et al., 2008) - Stable carbon isotope chemistry of bulk sediment or plant macrofossils in the range of mangrove environments (e.g., $-25 > \delta^{13}C > -28$; e.g., Khan, 2014) or plant tissue ($-26 > \delta^{13}C > -31$; e.g., Wooller et al., 2007)	(MTL + HAT)/2	HAT-MTL
Acropora palmata coral	- *In-situ* monospecific *Acropora palmata* framework (e.g., Toscano and Lundburg, 1998)	(MLLW-5)/2	5
Organic floodplain muds and peats	- Lithological description (e.g., Warne et al., 2002)	(MTL + HAT)/2	HAT-MTL
Microbial mat	- Lithological description (e.g., Knowles, 2008)	(MLLW + MHHW)/2	MHHW-MLLW
Beach rock	- Petrographic description of beach rock cement in thin section (e.g., aragonitic cement; Schubert et al., 1977) - Identifiable *in-situ* intertidal shells (e.g., species name; Schubert et al., 1977)	(MLW + HAT)/2	HAT-MLW
Marine limiting	- Identifiable *in-situ* intertidal shells (e.g., Klosowska, 2003) - Calcareous foraminiferal assemblage (e.g., Cheng et al., 2012) or diatoms dominated by marine taxa (e.g., Velez et al., 2014) -*In-situ* "deep water" corals, such as *Diplora* spp., *Orbicella* spp., and *Siderastrea* spp. (e.g., Gischler and Hudson, 2004) - Lithological description (e.g., *Halimeda* sand, Macintyre et al., 2004)	MTL	MTL
Terrestrial limiting	- Peat with freshwater macrofossils (e.g., Digerfeldt and Hendry, 1987) or stable carbon isotope chemistry of bulk sediment in the range of freshwater swamp environments (e.g., δ13C < −28; e.g., Khan, 2014)	MTL	> MTL

incorporated contaminating sources of older (e.g., dissolved CO_2 or HCO_3^- from radiocarbon-dead limestone) or younger (e.g., contemporary mangrove rootlets penetrating older sequences beneath the sediment surface) carbon. Following analysis by Hu (2010) of ^{14}C ages from bulk peat and plant macrofossils, a ±100 ^{14}C yr error was applied to bulk samples to account for sample contamination (Törnqvist et al., 2015). Many of these bulk samples were analyzed prior to the 1970s before correction of ^{14}C ages for isotopic fractionation became routine procedure (Stuiver and Polach, 1977; Törnqvist et al., 2015). We accounted for isotopic fractionation of $\delta^{13}C$ values (mangrove/freshwater plant tissue or peat: $-23 > \delta^{13}C > -31$‰; Vane et al., 2013; marine carbonates: $4 > \delta^{13}C > -4$‰; Stuiver and Polach, 1977; Polach, 1976) using a 4‰ (~64 ^{14}C yr) $\delta^{13}C$ uncertainty term. We corrected for this effect using the "dcorr" spreadsheet of the CALIB radiocarbon calibration program (available here: http://calib.qub.ac.uk/calib/fractionation.html). The total ^{14}C error was calculated as the quadratic sum of analytical (measurement) error, bulk error, and isotopic fractionation error (Törnqvist et al., 2015) (Table 2).

All corrected ^{14}C radiocarbon ages (and associated total error) were calibrated to sidereal years before present with a 2σ confidence interval and laboratory multiplier of 1 using the IntCal13 and Marine13 calibration curves (Reimer, 2013) for terrestrial (mangrove and freshwater) and marine samples (marine gastropods and corals), respectively. To account for the effect of local variations in marine reservoir age of dated marine carbonate samples, we used reservoir correction (ΔR) values from the Marine Reservoir Correction database (http://calib.qub.ac.uk/marine/) where available. Ages are presented as thousands of calibrated years before present (ka), where the zero point is 1950 CE (Stuiver and Polach, 1977).

2.2.2. U–Th age recalculation and screening

Ages of 55 samples in the database were obtained from corals dated using the U–Th method. U–Th dates were measured by thermal ionization mass spectrometry (TIMS) or multiple collector-inductively coupled plasma-mass spectrometry (MC-ICP-MS). We used the decay constants reported by Cheng et al. (2013) for ^{230}Th and ^{234}U and by Jaffey et al. (1971) for ^{238}U to recalculate U–Th ages and 2σ uncertainties and screened U–Th data for open-system behavior. This recalculation allows for direct comparison of data generated with different decay constants over the last several decades, but can only be performed for samples in studies where the measured activity ratios were reported. The effect of this recalculation on the reported age is typically small for samples of Holocene age relative to their originally published ages (here the difference in age ranges from 12 to 239 years) and is smallest for the youngest samples.

The sample age was excluded from further analysis if measured activities were unable to be obtained (n = 17), precluding age recalculation, or if one of the following criteria were not met (n = 5): (i) open-system behavior indicated by $\delta^{234}U$ within 10‰ of modern seawater (147‰), or (ii) diagenetic alteration indicated by <2% calcite (if mineralogy was reported) (Table 3).

Table 2
Age errors applied to Caribbean sea-level data.

Source of error	Description
Radiocarbon	
Laboratory error	1σ error provided by radiocarbon facility
Isotopic fractionation	When necessary: - Mangrove plant tissue and peat: −27 ± 4‰ - Marine carbonate: 0 ± 4‰
Bulk error	±100 years (Hu, 2010; Törnqvist et al., 2015)
Marine reservoir effect	ΔR and ΔR error taken from Marine Reservoir Correction Database
U-Th	
Laboratory error	2σ measurement error
Half-lives	Recalculated using Cheng et al. (2013) decay constants
Screening criteria	i) $\delta^{234}U$ within 10‰ of modern seawater (147‰) ii) <2% calcite (if mineralogy was reported) iii) ^{232}Th < 2 ppb (if reported)

We also screened for detrital Th (^{232}Th) content for samples where ^{232}Th concentration was reported. There were only 4 samples from St. Croix (Burke et al., 1989; Macintyre et al., 2008; Toscano et al., 2011) that have high ^{232}Th concentrations (ranging from 5 to 28 ppb) with corresponding back-calculated ^{230}Th/^{232}Th activity ratios <25. All of the remaining samples have ^{232}Th concentrations <2 ppb and ^{230}Th/^{232}Th activity ratios in the range of 700–30,000. Instead of rejecting these 4 samples from St. Croix, they were retained in the analysis using ^{232}Th-corrected ages assuming a bulk earth composition of the contaminating source, and correspondingly increasing the error associated with these ages. See Appendix 1 for measured activity ratios of all U–Th dated corals.

2.3. Estimation of relative sea level and its uncertainty

RSL is estimated using the equation (Shennan and Horton, 2002):

$$RSL_i = A_i - RWL_i$$

where A_i and RWL_i are the altitude and the reference water level of sample *i*, which are both expressed relative to MSL. In most cases, A_i was determined by measuring the depth of a sample in a core where the altitude of the core-borehole was known, although for a small number of samples, the altitude of submerged samples collected from outcrops was determined by direct measurement of its water depth (e.g., Robbin, 1984). All index points in the database are expressed relative to MSL, and negative values indicate RSL below present (0 m).

Sample-specific errors were calculated for each index point (Shennan and Horton, 2002). In addition to the indicative range, vertical errors were incorporated related to the indicative meaning of a sample, sampling errors, and measurement of a sample's altitude. A complete list and description of vertical errors is provided in Table 3. The total 2σ errors were calculated as the quadratic sum of individual sources of errors. Special consideration is given to uncertainties associated with sediment compaction and tectonic influences, both of which result in an upward or downward displacement of the altitude at which a sample was originally deposited, and to changes in the distribution of sea-level indicators over time due to Holocene changes in tidal range.

2.3.1. Sediment compaction

To account for the uncertainty of RSL due to sediment compaction, we subdivided the database into basal and intercalated categories (Shennan and Horton, 2002; Horton and Shennan, 2009). Basal samples are those recovered from within the sedimentary unit that overlies an incompressible substrate. Intercalated samples are derived from sediments that are interleaved between higher-density clastic sedimentary units; these samples are the most prone to compaction (Jelgersma, 1961). We assessed the relationship between sediment compaction and stratigraphic measurements such as overburden thickness (thickness of the column of sediment lying above the index point), depth to basement (thickness of the sequence between the index point and incompressible surface) and the total thickness of the sedimentary sequence (Shennan et al., 2000b; Edwards, 2006; Törnqvist et al., 2008; Horton and Shennan, 2009; Horton et al., 2013).

We selected two sites (Jamaica and Belize Central Barrier Reef) that have good temporal distribution of basal and intercalated index points to examine the relationship between sediment compaction and overburden thickness, depth to basement and the total thickness of the sedimentary sequence. We constructed Gaussian Process regression models of RSL conditioned upon the basal index points for each site using a Matérn covariance function with a smoothness parameter of 3/2 (Rasmussen and Williams, 2006). We then calculated the residuals between each intercalated index point and the predicted RSL from the models, based on the basal index points (Fig. 3a). A statistically significant linear relationship ($p < 0.001$) was found with overburden thickness (Fig. 3b), with a linear correlation coefficient of 0.70. We used the regression coefficient (0.22 ± 0.07 m of compaction per meter of overburden) to alter (i.e., shift up) the mean altitude of intercalated index points. An additional bidirectional error was added to the sample so the lower bound of RSL remained unchanged (Fig. 3c).

Table 3
Sources of vertical error considered for Caribbean sea-level data following database protocol of Hijma et al. (2015). MTL = mean tide level; MLLW = mean lower low water; MHHW = mean higher high water; HAT = highest astronomical tide; RSL = relative sea level; IR = indicative range; DEM = digital elevation model.

Source of error	Description
Indicative range (m)	Half the indicative range (IR)
Reference water level error (m)	0.1 m, based on a comparison of predictions from the tidal model (Fig. 4a) for 41 tide gauge locations in the Caribbean of the IR for mangroves (MTL to HAT), *A. palmata* corals (MLLW-5m to MLLW), microbial mats (MLLW to MHHW) and beach rock (MLLW to HAT) with the measured values at those tide gauge stations (Figure S2).
Indicative range error (m)	20% of the modern IR estimated from the average difference between the modeled and measured IR.
Indicative range change error (m)	Half the difference between the modern IR and the paleo-IR (see Section 2.3.2 for further explanation).
Sample thickness error (m)	Half the thickness of the sample (Shennan, 1986)
Sampling error (m)	±0.01 m, following Shennan (1986).
Core shortening/stretching error (m)	±0.15 m for rotary coring and vibracoring, ±0.05 m for hand coring (Woodroffe, 2006) and ±0.01 m for a Russian sampler (Woodroffe, 2006).
Non-vertical drilling error (m)	0.02 m/m depth. This error is unidirectional and makes the upward portion of the total vertical error larger than thedownward portion.
Tidal error (m)	Half the tidal range (Shennan, 1989); applies only to samples collected offshore with reference to the water surface.
Vegetation zone error (m)	±0.5 m; applies only to samples where land surface elevation was estimated using vegetation zones
Water depth error (m)	±0.5 m standard error used if not specified by the authors.
Map error (m)	Half contour line interval when used.
Leveling error (m)	0.01 m when leveling with high-precision (e.g., total station) equipment; ±0.03 m if leveling method is unknown (Törnqvist et al., 2004).
dGPS error (m)	±0.1 m standard error if not otherwise specified by the authors.
Uniform error adjustment (m)	Coral data follows a uniform distribution, so we convert to an approximate normal distribution by multiplying the standard deviation by $2\sqrt{3}$.
Compaction correction (m)	Intercalated data is adjusted by shifting the mean upwards by a factor of 0.22 m per m overburden thickness, and adding the difference between the new mean and the original minimum to the upward error.

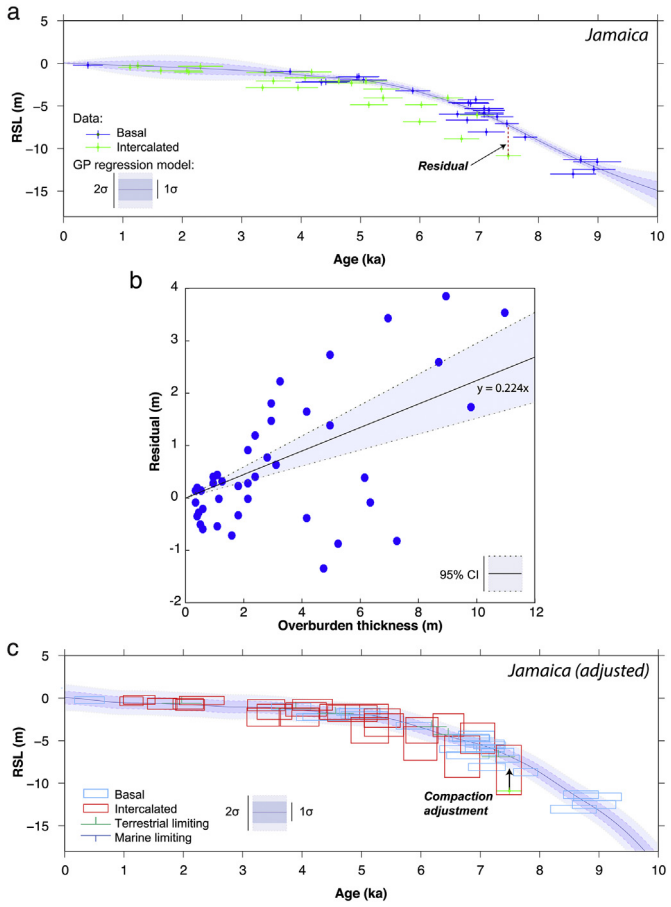

Fig. 3. Approach employed to account for sediment compaction of intercalated index points using Jamaica and the Central Belize Barrier Reef datasets. (a) Gaussian process (GP) regression model fit to basal index points. (b) Linear regression (with 95% confidence interval shown) of residuals between intercalated index points and GP model (calculated in a) and overburden thickness from both the Jamaica and Central Belize Barrier Reef datasets. This model is statistically significant at the 95% confidence level (with a coefficient of determination of 0.49, $p < 0.001$). (c) Adjusted intercalated sea-level data. The regression coefficient (calculated in b) was used to shift the midpoint of intercalated index points upward; an additional unidirectional error proportional to the regression coefficient was added in the downward direction to keep the lower bound of intercalated index points unchanged.

This addition of error accounts for the possibility that samples may not have been affected by the compaction process or more likely, that variation exists across sites in sediment lithology or other factors influencing compaction.

2.3.2. Tidal range change

Paleotidal data for the Caribbean were predicted using a nested modeling approach (Fig. 4). Complete details of the approach are available in Hill et al., 2011; Griffiths and Hill, 2015. First, a global tidal model (Griffiths and Peltier, 2008, 2009), which includes dynamics such as self-attraction and loading, drag in shallow seas, and internal tide drag, was used to compute tidal constituent amplitudes and phases on a 800 × 800 regular grid. These tidal constituents from the global model were used to force the open boundary of a regional tidal model (ADCIRC; Luettich and Westerink, 1991) using an unstructured finite-element computational mesh spanning the western Atlantic Ocean, the Gulf of Mexico and the Caribbean Sea. This model pairing is referred to as the 'paleotidal model' (Fig. 4b). Paleobathymetries were estimated from depth changes from the ICE−5G (VM2) GIA model of Peltier (2004) interpolated onto the regional grid. Tidal amplitudes and phases were converted to tidal datums using the Harmonic Constant Datum method of Mofjeld et al., 2004. The paleotidal model does not include the effects of sediment infilling of estuaries and coastal lowlands or freshwater discharge from the catchments (Shennan et al., 2000a).

An error was applied to all index points to account for the local tidal conditions that prevailed at the time of sample deposition using hindcasts from the paleotidal model. Computational runs were carried out at 1 ka intervals from 10 ka to present day. We followed Hill et al. (2011) and Horton et al. (2013) to determine absolute values of past tidal levels. The percentage change in each tidal datum between present day (Fig. 4b) and paleotidal model runs at the time of interest (Fig. 4d) was used to correct the present-day tidal datums produced by the regional model forced with tidal constituents from the data-assimilative TPXO 6.2 global model (Egbert et al., 1994) (Fig. 4a), which more accurately reproduces present-day tidal datums recorded at tide gauges. An additional error was added to each index point equal to the absolute value of the difference between present-day and past indicative range of the sample (calculated from model output) (Table 3). Barbados and South American sites were outside of the domain of the paleotidal model and therefore data from these sites were not corrected for this effect.

Here, we provide a brief example of how this calculation was made for an index point. The present-day indicative range for a mangrove peat sampled from Swan Key in the Florida Keys is:

$$\text{HAT - MTL} = 0.64\ \text{m} - 0.01\ \text{m} = 0.65\ \text{m}$$

The sample was dated to 5.5 ka. The paleotidal model was used to provide estimates of MTL and HAT and the 'paleo' indicative range was calculated:

$$\text{HAT - MTL} = 0.70\ \text{m} - 0.01\ \text{m} = 0.71\ \text{m}$$

The absolute difference between the present-day and 'paleo' indicative range (0.06 m) was incorporated as a term in the total quadratic sum of vertical errors of RSL. The magnitude of this indicative range change error is small (<0.1 m) from 8 to 0 ka., although for a few index points, the magnitude of this error increases to as much as ~0.55 m from 10 to 8 ka (Fig. 4c). By adding an error term, instead of directly correcting for this effect, we are incorporating the best estimate of the uncertainty inherent in the RSL reconstructions due to past changes in tidal range (Hijma et al., 2015).

2.3.3. Tectonic influences in the Caribbean

To minimize the uncertainties in RSL due to tectonic influence on sites, we have excluded studies that documented gradients of RSL change across active tectonic structures (e.g., Ignacio Martínez et al., 2010). Indeed, most sites within the database (with the exception of Jamaica, Dominican Republic, Belize) lie tens of kilometers away from large active faults and are, therefore, unlikely to experience short-term vertical displacements greater than a few centimeters (e.g., Rundle, 1982; Yu et al., 1996). Only the Caribbean subduction zone could potentially produce earthquakes large enough to produce larger vertical displacements in the far field (>M8); however, no such earthquakes are known from historical records (Bernard and Lambert, 1988), either because the historical record is too short to capture them, or because the Caribbean subduction zone does not generate them. If such great earthquakes were to occur, they could affect the records of the Lesser Antilles and Barbados sites. Documented long-term uplift rates exist for a small number of sites in the Caribbean: 0 m/Ma in Barbuda (Brasier and Donahue, 1985), 30 m/Ma along the northern coast of Puerto

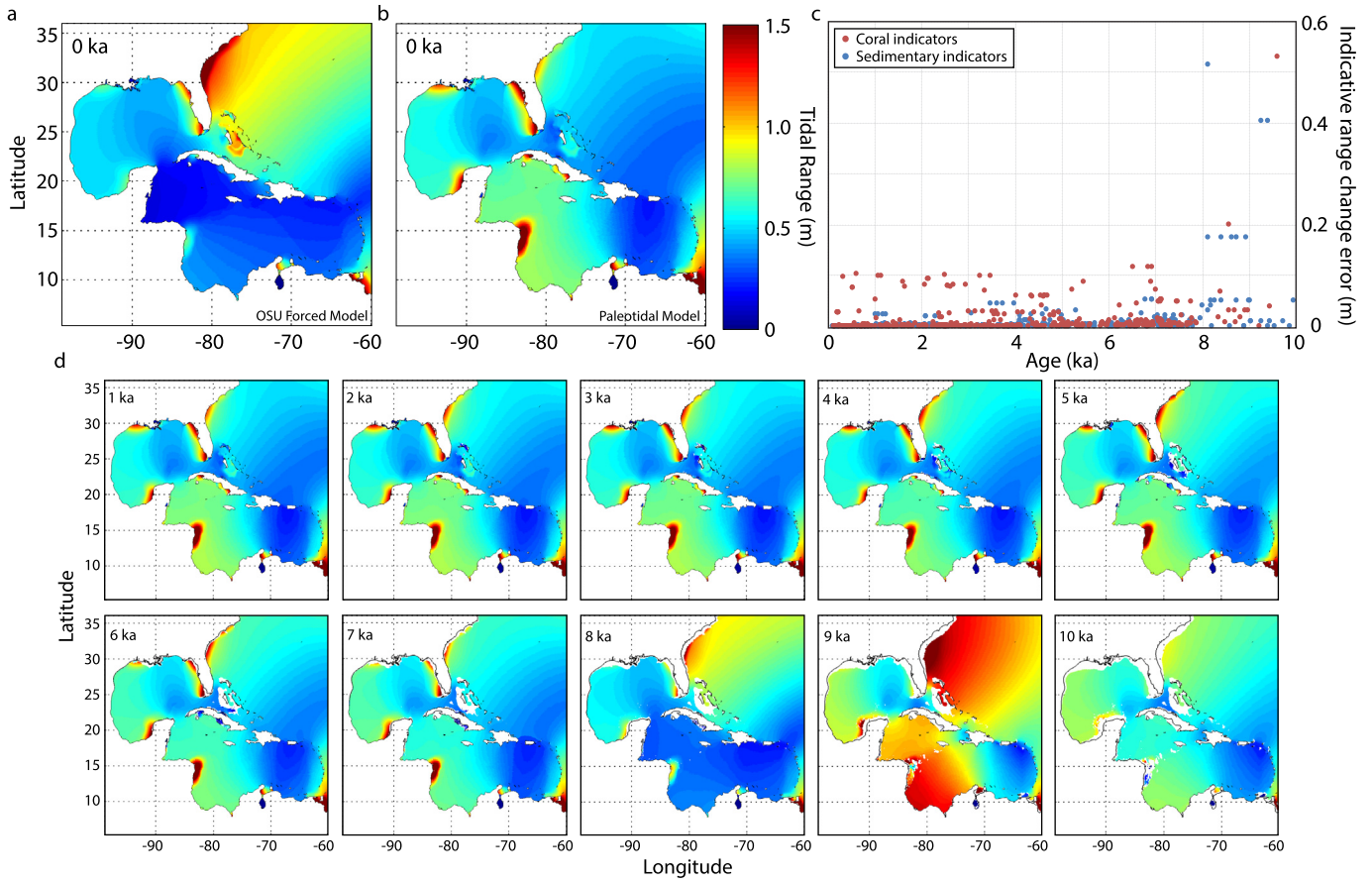

Fig. 4. Holocene change in Caribbean tides. (a) Present-day tidal range computed by OSU (Oregon State University) forced model. (b) Present-day tidal range computed by paleotidal model. (c) Magnitude of the uncertainty added to index points due to changes in tidal range over the past 10 ka. (d) Hindcasts of tidal range using paleotidal at 1-kyr intervals from 10 to 1 ka). MTL = mean tide level; MLLW = mean lower low water; MHHW = mean higher high water; HAT = highest astronomical tide.

Rico (Taggart, 1993), 25–60 m/Ma in the Cayman Islands (Vezina et al., 1999), 50 m/Ma in Florida due to erosional unloading by karstification of the emerged landmass (Adams et al., 2010), 26–54 m/Ma in Curacao (Muhs et al., 2012) and 340 m/Ma along the southern coast of Barbados (Fairbanks, 1989; Peltier et al., 2015). Given the large uncertainties of available uplift estimates (e.g., Creveling et al., 2015) and the limited number of sites for which this information is available, we do not use these estimates to correct the data and instead compare RSL heights and rates among sites to make inference on tectonic influences.

2.4. Statistical modeling of Holocene sea-level data

We construct a spatio-temporal empirical hierarchical model, which is suitable for analyzing noisy RSL time series from multiple locations (Kopp et al., 2016). In the sense we use it here, 'noise' refers to both uncertainties in measurements and high-frequency variability in sea level that may affect the observation process but should not be considered part of the multidecadal definition of mean sea level. The model has three levels: (1) a data level, $p(\mathbf{y}, \widehat{\mathbf{t}}|\mathbf{f}, \mathbf{t}, \widehat{\boldsymbol{\Theta}_\mathbf{d}})$, which models how RSL at specific points in space and time is recorded by index points with vertical and temporal noise; (2) a process level, $p(\mathbf{f}, \mathbf{t}|\widehat{\boldsymbol{\Theta}_\mathbf{p}})$, which models the noise-free spatio-temporal field of RSL, including basinal (uniform across the entire Caribbean basin), sub-basinal (exhibiting regional variability within the Caribbean basin), and local (exhibiting little spatial correlation) signals; and (3) a hyperparameter level ($\boldsymbol{\Theta} = [\boldsymbol{\Theta}_\boldsymbol{p}, \boldsymbol{\Theta}_d]$), (process-level and data-level hyperparameters), which characterize the spatial and temporal scales of variability in the process level. Here, $\mathbf{y}$ refers to a vector of RSL observations, $\widehat{\mathbf{t}}$ to a vector of age observations, $\mathbf{f}$ a vector of RSL at both observed and unobserved locations of interest, and $\mathbf{t}$ a vector of true ages corresponding to $\widehat{\mathbf{t}}$. The notation $p(a|b,c)$ reads the probability or probability density of a conditional on b and c.

We employ an empirical Bayesian analysis method, in which the hyperparameters are point estimates (single values with no associated probability distribution) calibrated on the data to maximize the likelihood of the model. The output of the model includes an estimate of the posterior probability distribution of the noise-free sea-level field, $f(x,t)$, conditional on the tuned hyperparameters:

$$p\left(\mathbf{f}, \mathbf{t}|\mathbf{y}, \widehat{\mathbf{t}}, \widehat{\boldsymbol{\Theta}_\boldsymbol{d}}, \widehat{\boldsymbol{\Theta}_\boldsymbol{p}}\right) \propto p\left(\mathbf{y}, \widehat{\mathbf{t}} \middle| \mathbf{f}, \mathbf{t}, \widehat{\boldsymbol{\Theta}_\mathbf{d}}\right) \cdot p\left(\mathbf{f}, \mathbf{t} \middle| \widehat{\boldsymbol{\Theta}_\mathbf{p}}\right)$$

The vector $\widehat{\boldsymbol{\Theta}_\boldsymbol{d}}$ is the maximum likelihood estimates of the data hyperparameter ($\boldsymbol{\Theta}_\boldsymbol{d} = \{\sigma_w^2\}$) and $\widehat{\boldsymbol{\Theta}_\boldsymbol{p}}$ is the maximum likelihood estimates of the process hyperparameters ($\boldsymbol{\Theta}_\boldsymbol{p} = \{\sigma_b^2, \tau_b, \sigma_s^2, \gamma_s, \tau_s, \sigma_l^2, \gamma_l, \tau_l\}$). These hyperparameter point estimates $\widehat{\boldsymbol{\Theta}}$ are detailed in Appendix 2.

At the data level, we have noisy RSL measurements y_i and noisy age measurements $\widehat{t}_i$:

$$y_i = f(\mathbf{x}_i, t_i) + \varepsilon_i^y$$

$$\widehat{t_i} = t_i + \varepsilon_i^t$$

where $\mathbf{x}_i$ is the geographic location and t_i is the true (noise-free) age of index point i; $\widehat{t_i}$ are the midpoints of calibrated ages; ε_i^y are the errors in the RSL; and ε_i^t are errors in age. The RSL errors are treated as uncorrelated and normally distributed (where *Acropora palmata* coral's uniform distribution is approximated with a normal distribution; see Table 3), with standard deviations equal to half the quadratic sum of each measurement's heteroscedastic (unequal variability across index points) total error (as described in section 3.3 and Table 2) and an additional homoscedastic (equal variability) noise with standard deviation σ_w, representing high-frequency variability in RSL. The non-normal age uncertainties (described in section 3.2 and Table 3) are approximated as 2σ Gaussian uncertainties and are incorporated using the noisy-input Gaussian Process (GP) method of McHutchon and Rasmussen (2011), which uses a first-order Taylor-series approximation to translate errors in the independent variable (age) into equivalent errors in the dependent variable (RSL):

$$f(\mathbf{x}_i, t_i) \approx f\left(\mathbf{x}_i, \widehat{t_i}\right) + \varepsilon_i^t \frac{\partial f\left(\mathbf{x}_i, \widehat{t_i}\right)}{\partial t}$$

At the process level, the model uses spatial and temporal covariance that exists among the data to reduce uncertainty in estimates of the posterior sea-level field. In many cases the model uncertainty is less than the uncertainty of a single index point at a single site. Likewise, the model allows us to estimate the sea-level field for locations and at times where there is no data. We model the sea-level field, $f(\mathbf{x},t)$, as the sum of three (basinal, sub-basinal, local) component spatio-temporal fields:

$$f(\boldsymbol{x}, t) = b(t) + s(\mathbf{x}, t) + l(\mathbf{x}, t).$$

This sum is equal to the total RSL signal at a given site (model curves shown in Figs. 5–8). The prior distribution of each component is a mean-zero GP, an infinite-dimensional generalization of multivariate normal distributions (see Rasmussen and Williams, 2006 for more detailed information on GPs). The covariance is characterized by hyperparameters that comprise amplitudes (σ; i.e., magnitude of signal), timescales (τ; i.e., time over which the sea-level field is correlated), and geographic length scales (γ; i.e., geographic distance over which the sea-level field is correlated) of variability for the basinal (denoted by subscript 'b'), sub-basinal (denoted by subscript 's') and local (denoted by subscript 'l') component fields. The priors for the basinal, sub-basinal, and local component fields are respectively defined by:

$$b(t) \sim GP\left\{0, \sigma_b^2\, \rho\left(t, t'; \tau_{\boldsymbol{b}}\right)\right\}$$
$$s(\mathbf{x}, t) \sim GP\left\{0, \sigma_s^2\, \rho\left(x, x'; \gamma_r\right)\rho\left(t, t'; \tau_s\right)\right\}$$
$$l(\mathbf{x}, t) \sim GP\left\{0, \sigma_l^2\, \rho\left(x, x'; \gamma_l\right)\rho\left(t, t'; \tau_l\right)\right\},$$

where ρ is the Matérn correlation function with smoothness parameter 3/2 and scale τ or γ (temporal or length, respectively). The use of a smoothness parameter of 3/2 ensures that the first derivative of the process will be defined everywhere, which allows for rates of RSL change to be calculated analytically (without estimation or approximation) over space and time.

The reported rates of sea-level change are 1-ka average rates based on a linear transformation of $f(t)$, unless otherwise stated. In the following sections, we present model predictions and rates using the mean and 1σ uncertainty. In order to assess the probability of a highstand geographically, we calculate the probability that RSL is greater than zero (current RSL), at grid points on the map over specific ranges in time.

3. Regional records of Caribbean relative sea-level

The new database incorporates sea-level data from a latitudinal range of 5°N to 25°N and longitudinal range of 55°W to 90°W (Fig. 1). The database consists of 737 data points, of which 499 are index points, 203 are marine limiting, and 35 are freshwater limiting dates. Most of the data are distributed temporally in the last 8 ka (90%), with the greatest amount (~26%) occurring from 8 to 6 ka. This distribution differs from records from the U.S. Atlantic coast, where only 7% of the data is older than 6 ka (Engelhart and Horton, 2012). This difference may be related to the lower GIA subsidence rates in the Caribbean compared to the U.S. Atlantic coast (i.e., shallower depths of samples between 6 and 8 ka), which either contributes to better preservation of sea-level indicators or samples that are easier to be obtained.

We subdivide the data into 20 regions based on availability of data, tectonic setting, and distance from the former LIS (Fig. 5: Western Antilles; 6: Eastern Antilles; 7: Florida and Central America; and 8: South America). In this section, we present past RSL and age of index points from values in the database for which tidal range change and sediment compaction are accounted in the error term. We report 2σ errors for RSL uncertainties and for clarity, we describe ages to the nearest 0.1 ka without chronological uncertainty. We include results from the spatio-temporal statistical model to indicate 1-ka average rates of change over specified time intervals. All RSL data used in this study can be found in Appendix 3.

3.1. Bahamas

The Bahamas RSL record contains 16 index points from mangrove peats (n = 11) and *A. palmata* corals (n = 5) and 17 marine limiting dates (Fig. 5.1). There is an absence of early Holocene data from the Bahamas. Index points from *A. palmata* corals (Lighty et al., 1982) and mangrove peats (Knowles, 2008) constrain the mid to late Holocene RSL record. The oldest index point (Andersen and Boardman, 1988) places RSL at −5.6 ± 0.7 m at 7 ka (midpoint), although this index point has a large age error (±2430). At 4.7 ka, an index point from an *A. palmata* coral indicates RSL was at −3.9 ± 2.8 m. The record shows RSL slowly rising to present at a rate of 0.9 ± 0.2 m/ka, with the youngest index point delimiting RSL to be −1.0 ± 1.2 m at 0.2 ka.

3.2. Cuba

The RSL record from Cuba is based on 5 index points from *Rhizophora mangle* and *Avicennia germinans* mangrove peats (Fig. 5.2). The record spans only the late Holocene (Peros, 2005; Davidson, 2007; Milne and Peros, 2013). The oldest index point places RSL at −2.7 ± 0.5 m at 2.5 ka. RSL then rose to −0.7 ± 0.6 m at 0.3 ka at a rate of 0.5 ± 0.4 m/ka.

3.3. Cayman Islands

The Cayman RSL history is defined by 9 index points from mangrove peat and 1 marine limiting date (Fig. 5.3). The oldest marine limiting date comes from a *Diploria labyrinthiformis* coral from a relict reef crest (Blanchon et al., 2002), which indicates RSL was above −22.0 ± 0.4 m by 6.1 ka. There is a gap in the record in the mid Holocene. The late Holocene record is constrained by index points from basal mangrove peats (Woodroffe, 1983). These index points show RSL at −1.5 ± 0.2 m at 2.1 ka increasing gradually at a

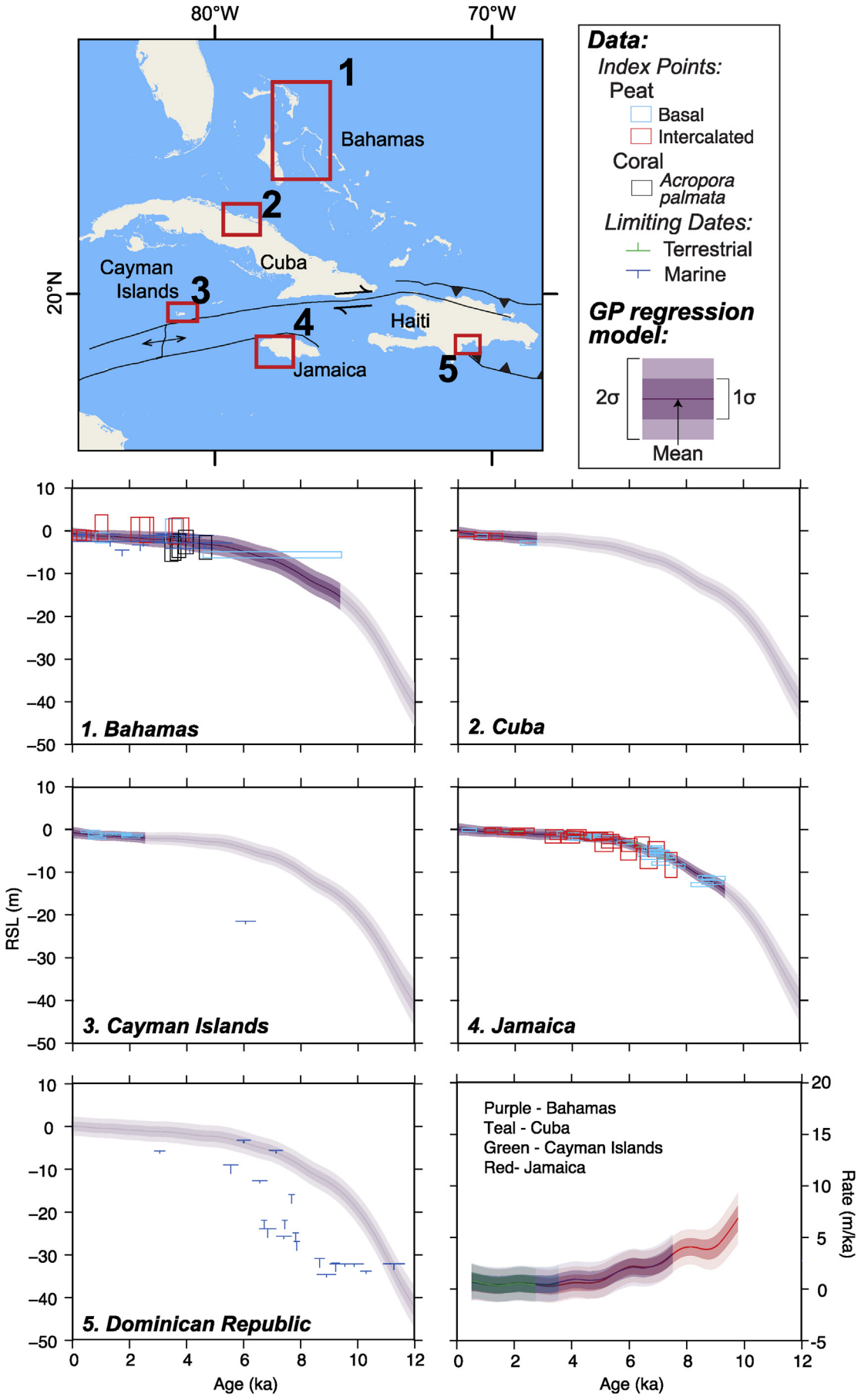

Fig. 5. RSL data and spatio-temporal statistical model predictions for the Western Antilles. (1) Bahamas; (2) Cuba; (3) Cayman Islands; (4) Jamaica; and (5) Dominican Republic.

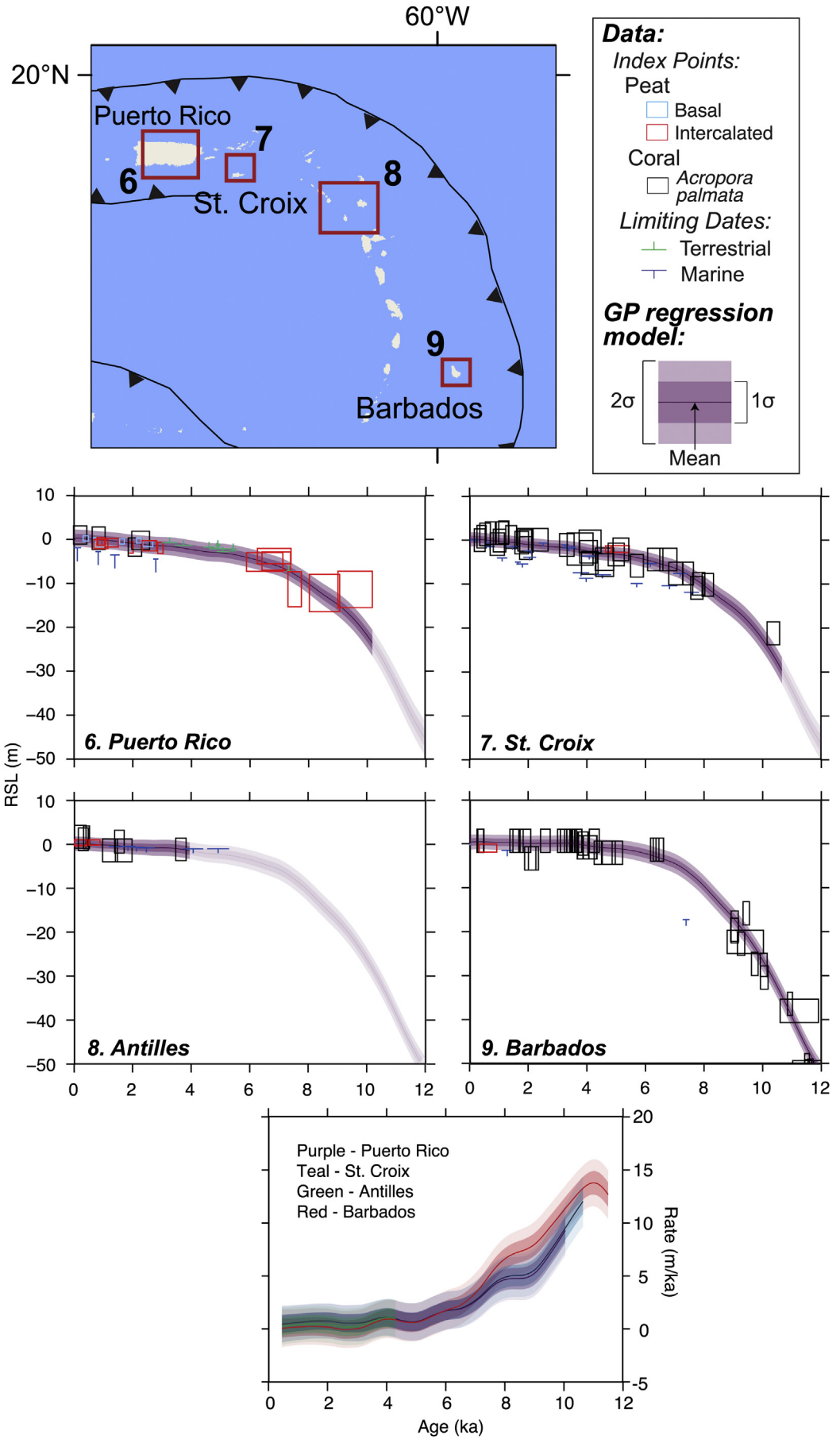

Fig. 6. RSL data and spatio-temporal statistical model predictions for the Eastern Antilles. (6) Puerto Rico; (7) St. Croix; (8) Lesser Antilles: Antigua, Martinique, Barbuda; and (9) Barbados.

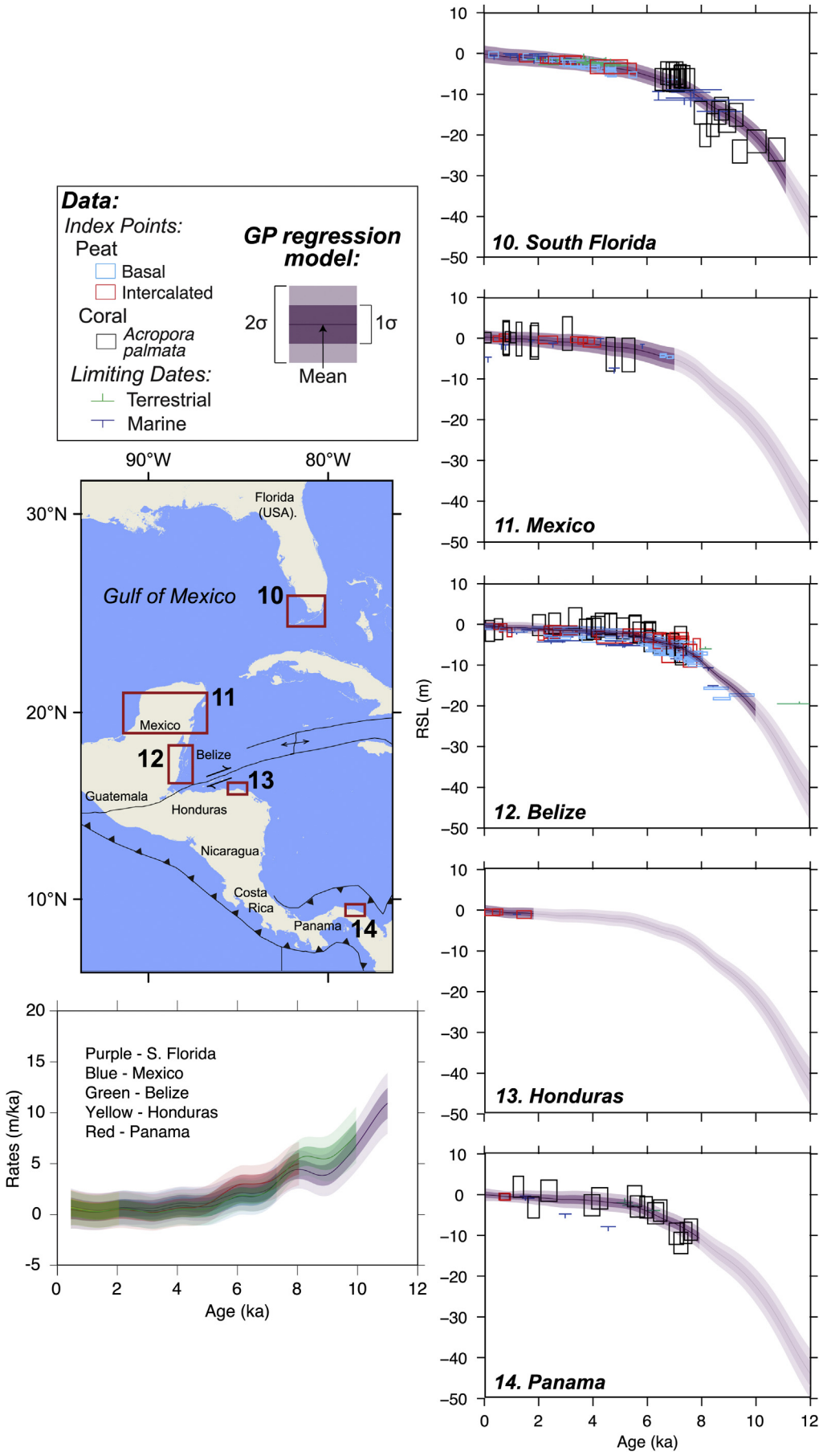

Fig. 7. RSL data and spatio-temporal statistical model predictions for Florida and the Central American coastline. (10) South Florida; (11) Mexico; (12) Belize; (13) Honduras; and (14) Panama.

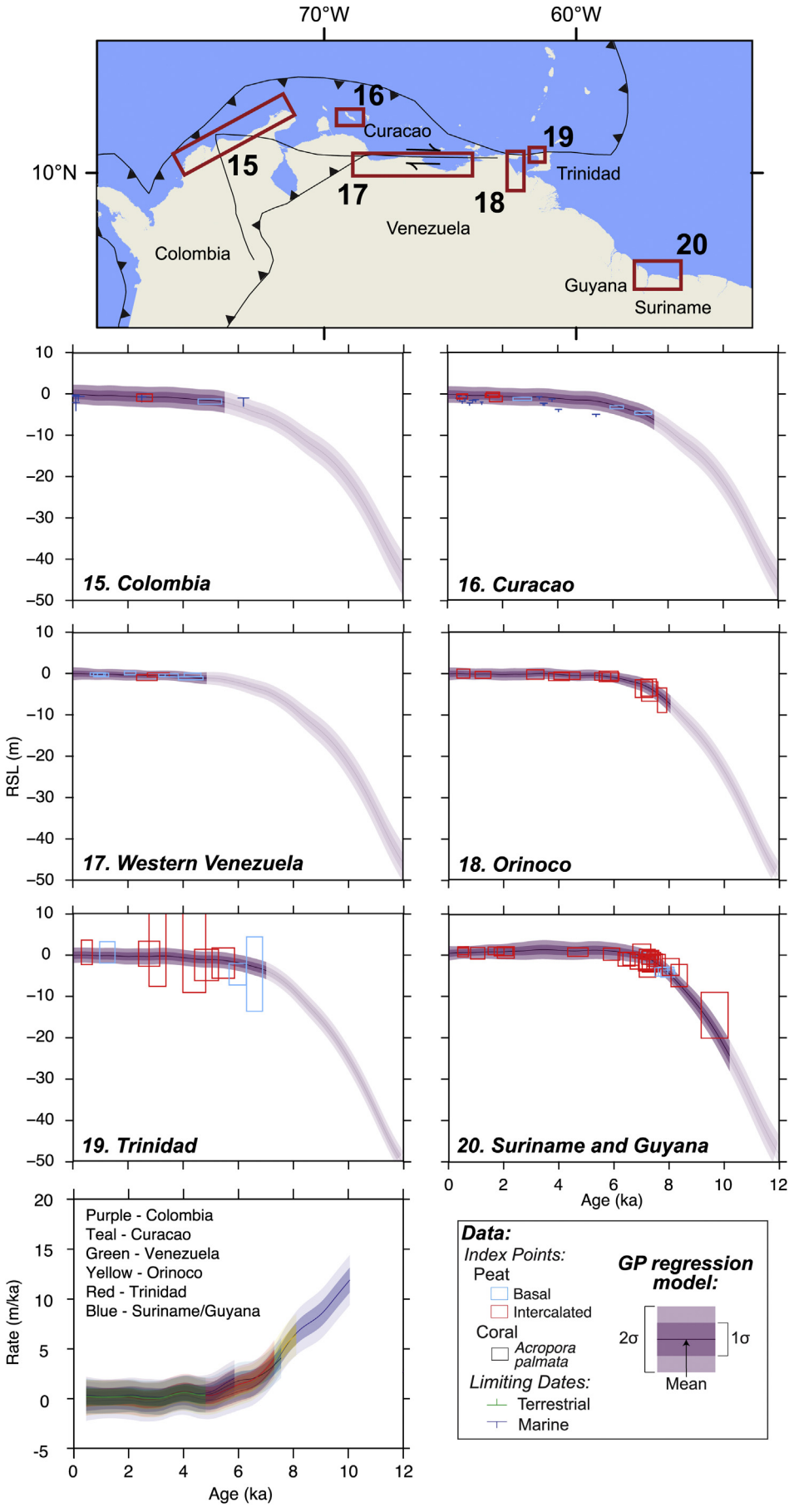

Fig. 8. RSL data and spatio-temporal statistical model predictions for the South American coastline. (15) Colombia; (16) Curacao; (17) Venezuela; (18) Orinoco; (19) Trinidad; and (20) Suriname and Guyana.

rate of 0.4 ± 0.5 m/ka to −0.6 ± 0.2 m at 0.5 ka.

3.4. Jamaica

The Jamaica database includes 49 index points from mangrove peat and 6 freshwater limiting dates (Digerfeldt and Hendry, 1987) (Fig. 5.4). The record spans most of the Holocene, with the oldest index point placing RSL at −11.6 ± 0.5 m at 9 ka. RSL increased rapidly at a rate of 2.7 ± 0.3 m/ka in the early to mid Holocene to −2.0 ± 0.4 m at 5 ka. RSL increased slowly at a rate of 0.4 ± 0.2 m/ka in the mid to late Holocene, with RSL reaching −0.2 ± 0.4 m at 0.4 ka.

3.5. Dominican Republic

The Dominican Republic contains 17 marine limiting points from exposed deep-water corals and mollusks in Lago Enriquillo (Mann et al., 1984; Taylor et al., 1985; Cuevas et al., 2009) (Fig. 5.5), which constrains a lower limit of RSL in the Holocene.

3.6. Puerto Rico

The RSL history of Puerto Rico is defined by 22 index points from mangrove peat (n = 18) and *A. palmata* corals (n = 4), 4 marine limiting dates and 10 freshwater limiting dates (Fig. 6.6). The early Holocene record is derived from mangrove peat index points (Shlemon and Capacete, 1976; Khan, 2014), the oldest of which constrains the position of RSL to be −12.2 ± 4.3 m at 8.6 ka. RSL rose rapidly at a rate of 2.7 ± 0.4 m/ka during the early to mid Holocene, reaching a maximum of −0.8 ± 0.6 m at 4.9 ka. The mid to late Holocene record is delimited by freshwater limiting points (Khan, 2014), with RSL at a maximum of −0.2 ± 0.6 m at 3.2 ka. The late Holocene record, defined by marine limiting dates (Lane et al., 2013) and index points from mangrove peat (Khan, 2014) and *A. palmata* (Macintyre et al., 1983) show RSL rising slowly at a rate of 0.6 ± 0.4 m/ka, reaching near its current level by 0.8 ka.

3.7. St Croix

The record from St. Croix consists of 34 index points from *A. palmata* corals (n = 32) and mangrove peat (n = 2) and 34 marine limiting dates (Fig. 6.7). Coral data from several St. Croix reef sites combine to provide comprehensive temporal (~8 ka) coverage of Holocene reef development (Burke et al., 1989; Macintyre and Adey, 1990; Hubbard et al., 2005; Macintyre et al., 2008; Toscano et al., 2011), with additional supporting information from marine limiting dates and mangrove peat index points from Altona Bay (Jessen et al., 2008). The oldest index point places RSL at −20.9 ± 2.6 m at 10.4 ka. RSL rose in the early (6.9 ± 0.6 m/ka) to mid (4.3 ± 0.3 m/ka) Holocene, reaching −10.4 ± 2.6 m at 8.1 ka and −3.5 ± 2.6 m at 5.0 ka. The rate of RSL rise slowed to 0.7 ± 0.2 m/ka in the mid to late Holocene, with the youngest index point indicating RSL was located at −0.2 ± 2.6 m at 0.3 ka.

3.8. Antilles

The record from the Lesser Antilles island arc, including sites in Anguilla, Antigua, Barbuda, and Martinique, contains 12 index points from *A. palmata* corals (n = 7) and microbial mats (n = 5) and 7 marine limiting dates (Fig. 6.8). We exclude mangrove peat data from Guadeloupe (Feller et al., 1990) because the age and altitude of dated samples could not be accurately estimated. The Antilles dataset has limited temporal coverage, with marine limiting dates and index points from microbial mats in coastal lagoons from Anguilla and Barbuda (Knowles, 2008) and *A. palmata* corals (Adey and Burke, 1976; Lighty et al., 1982; Macintyre et al., 1985) defining the position of RSL in the mid to late Holocene. The oldest marine limiting date places the lower limit of RSL at −1.4 ± 0.5 m at 4.9 ka, with a slow rise of 0.5 ± 0.2 m/ka to the present-day level.

3.9. Barbados

The RSL history of Barbados is derived from 54 index points from *A. palmata* corals (n = 52) and mangrove peat (n = 1) and 13 marine limiting dates (from deep water corals) (Fig. 6.9). The early Holocene record is constrained by an expanded dataset (Fairbanks et al., 2005; Peltier and Fairbanks, 2006) of the landmark Barbados deglacial RSL history described in Fairbanks (1989, 1990) and Bard et al. (1990, 1993, 1998), where U-series ages have been re-measured on some of the same samples with improved precision (Fairbanks et al., 2005). The mid to late Holocene record is derived from index points from *A. palmata* collected from Cobbler's Reef, a well-developed bank-barrier reef off the southeast coast (Macintyre et al., 2007a, 2007b), and mangrove peat from Graeme Hall swamp on the south coast of Barbados (Ramcharan, 2005). RSL rose rapidly at a rate of 12.8 ± 0.7 m/ka in the early Holocene from −54.6 ± 2.6 m at 12 ka to −30.3 ± 2.6 m at 10 ka. A steady rise of 9.5 ± 1.1 m/ka continued to 9 ka when RSL reached −18.8 ± 2.6 m. There is a gap in the record until 6.5 ka with only one marine limiting date indicating the lower limit of RSL to be −17.8 ± 0.7 m at 7.4 ka. In the mid to late Holocene, RSL rose at a slower rate (0.6 ± 0.2 m/ka) from −1.2 ± 2.6 m at 6.5 ka to its present day level.

3.10. Southern Florida, USA

The RSL history from the southern Florida is composed of 52 index points from mangrove peats (n = 30) and *A. palmata* corals (n = 22), 26 marine limiting dates (deep water corals) and 16 freshwater limiting dates (Fig. 7.10). Index points from *A. palmata* and marine limiting dates along the Florida reef tract delimit the early Holocene position of RSL (Lighty et al., 1978; Toscano and Lundberg, 1998; Toscano and Macintyre, 2003; Banks et al., 2007); RSL rose rapidly (4.3 ± 0.5 m/ka) during this time from −21.6 ± 2.8 m below present at ~10 ka to −6.4 ± 2.7 m at ~ 7 ka. An index point from mangrove peat indicates RSL was at −5.2 ± 0.7 m at 5.5 ka. The mid to late Holocene record is defined by index points from mangrove peat (Scholl, 1964; Scholl and Stuiver, 1967; Robbin, 1984) and marine limiting dates (Cheng et al., 2012) that place RSL between −2.5 and −5.5 m at 4.5 ka. RSL rose slowly at a rate of 0.7 ± 0.3 m/ka to present, with the youngest index point indicating RSL to be at −0.3 ± 0.7 m at 0.3 ka.

3.11. Mexico

Mexico's RSL history is constrained by 21 index points from *A. palmata* corals (n = 11) and mangrove peat (n = 10) and 8 marine limiting dates (Fig. 7.11). There is a lack of data until 6.9 ka when index points from mangrove peat formed within Cenote Aktun Ha (Gabriel et al., 2009) indicate RSL was between −3.6 and −4.8 m from 6.9 to 6.6 ka. The mid to late Holocene record is constrained by marine limiting points and index points from *A. palmata* corals (Blanchon et al., 2002) and mangrove peat (Islebe and Sánchez, 2002; Torrescano and Islebe, 2006; Torrescano-Valle and Islebe, 2012; Gutiérrez-Ayala et al., 2012) and shows a gradual rise of 0.4 ± 0.3 m/ka from −1.0 ± 1.1 m at 4.0 ka to present-day level.

3.12. Belize

Belize has the largest amount of data among all sites. These data consist of 137 index points, 45 marine limiting dates and 2

terrestrial limiting dates from the northern barrier reef, central barrier reef, southern barrier reef, Turneffe Islands and Lighthouse/Glover's reef (Fig. 7.13). Local to regional tectonics may influence local Belize RSL histories (Lara, 1993), although no large offsets were observed among localities, so we combine data from this region. The RSL record from the Belize barrier reef consists of 28 marine limiting dates and 116 index points from mangrove peat (n = 98) from Ambergris Cay (Ebanks, 1967), Cangrejo and Bulkhead Shoal (Mazzullo et al., 2003), Tobacco Range (Macintyre et al., 1995); Twin Cays (Macintyre et al., 2004; McKee et al., 2007; Wooller et al., 2007), Cat Cay (McKee et al., 2007) and Spanish Lookout Cay (Monacci et al., 2009) and *A. palmata* corals (n = 18) from Gladden Spit, Ranguana Cay, and Nicholas Cay (Gischler and Hudson, 2004). The RSL history from the Turneffe Islands and Lighthouse/Glover's reef is derived from 17 marine limiting dates and 21 index points from *A. palmata* corals (n = 6) (Gischler and Hudson, 1998) and mangrove peat (n = 15) (Gischler and Hudson, 1998; Gischler, 2003; Wooller et al., 2009; McCloskey and Liu, 2013), and 2 terrestrial limiting dates (Gischler, 2003). The oldest index point constrains the position of RSL to be −17.3 ± 0.3 m at 9.4 ka. RSL then rose at 4.0 ± 0.4 m/ka in the early Holocene, reaching a level of −2.1 ± 2.6 m at 6.1 ka. RSL rise slowed to 0.5 ± 0.2 m/ka at this time, reaching a value of −0.5 ± 0.6 m by 0.6 ka.

3.13. Honduras

The RSL record from Honduras is based on 3 index points from mangrove peat and 1 marine limiting date (McKee et al., 2007) (Fig. 7.13). There is limited temporal coverage of this record, with the oldest index point placing RSL at −1.3 ± 0.9 m at 1.4 ka. RSL then rose at a rate of 0.5 ± 0.6 m/ka to the present level.

3.14. Panama

The RSL history from Panama is composed of 16 index points from mangrove peats (n = 2) (Schmidt, 2008) and *A. palmata* corals (n = 14) (Macintyre and Glynn, 1976), 6 marine limiting dates from deep-water corals (Macintyre and Glynn, 1976) and marine-influenced lagoonal deposits (Schmidt, 2008), and 3 freshwater limiting dates (Schmidt, 2008) (Fig. 7.14). Panama displays a monotonic rise in RSL, with sea level rising at a rate of 3.0 ± 0.6 m/ka from −9.6 ± 2.6 m at 7.4 ka to −3.1 ± 2.6 m at 5.6 ka BP. From ~4 ka, the rate of RSL rise decreased to 0.3 ± 0.3 m/ka, with RSL increasing from −1.1 ± 2.6 m at 4.2 ka to −0.7 ± 0.8 m at 0.7 ka.

3.15. Colombia

The Colombian record contains 2 index points from mangrove peat (Jaramillo and Bayona, 2000) and 7 marine limiting points (González et al., 2010; Urrego et al., 2013) (Fig. 8.15). We did not include data from Ignacio Martínez et al. (2010) and Velez et al. (2014) in the database due to obvious tectonic influences and unknown sample elevation and indicative meaning. The oldest marine limiting date indicates RSL was above −1.5 ± 1.1 m at 6.2 ka. RSL then remained at a relatively constant level until present, reaching −1.9 ± 0.6 m at 5.0 ka, rising slightly (0.3 ± 0.5 m/ka) to −0.9 ± 0.9 m at 2.6 ka.

3.16. Curaçao

The Curaçao database contains 8 index points from mangrove peat and 17 marine limiting dates (Klosowska, 2003) (Fig. 8.16). The record begins at 7.1 ka, where a single index point places RSL at −4.7 ± 0.4 m. RSL then rose at a rate of 2.1 ± 0.9 m/ka to −3.3 ± 0.4 m at 6.1 ka. The mid to late Holocene record is constrained only by a series of marine limiting dates, which indicate RSL rose at a rate of 0.7 ± 0.4 m/ka to above −1.1 ± 0.3 m by 3.3 ka. RSL then rose slowly (0.2 ± 0.6 m/ka) to −0.5 ± 0.4 m at 1.7 ka and to above −0.6 ± 0.3 m at 0.4 ka.

3.17. Western Venezuela

We separate the record of western Venezuela from the Orinoco Delta region due to differing tectonic influences. Western Venezuela's RSL record consists of 10 index points from mangrove peat (n = 6) (Weiss, 1979) and beach rock (n = 4) (Schubert et al., 1977) (Fig. 8.17). The western Venezuelan record begins in the mid Holocene, with the oldest index point placing RSL at −0.3 ± 0.4 m at 4.4 ka. RSL then rose slowly at 0.2 ± 0.3 m/ka until it reached −0.1 ± 0.4 m at 0.9 ka. We note, however, that we excluded beach rock samples found up to 2 m above present (Schubert et al., 1977) RSL because the dated material was not formed *in situ*. The presence of the beach rock features suggests that RSL may have been higher than present in the recent (Holocene) past in this location. Further investigation is required to fully assess the possibility of a mid-Holocene highstand in this region.

3.18. Orinoco Delta

The RSL record from the Orinoco Delta on the eastern coast of Venezuela consists of 13 index points from mangrove peat and organic muds inferred to be buried A soil horizons (Rull et al., 1999; Warne et al., 2002) (Fig. 8.18). The Orinoco record has good temporal coverage over the past ~8 ka. The record shows rapid RSL rise (2.7 ± 0.6 m/ka) in the early to mid Holocene. RSL rose from −6.8 ± 3.0 m at 7.8 ka to −1.0 ± 0.9 m by 5.9 ka. The position of RSL remained relatively constant throughout the mid to late Holocene, rising slowly at a rate of 0.2 ± 0.2 m/ka to −0.3 ± 1.1 m by 0.5 ka.

3.19. Trinidad

The RSL history from Trinidad is derived from 9 index points from mangrove peat (Ramcharan and McAndrews, 2006) (Fig. 8.19). The Trinidad record displays a monotonic rise in RSL, with faster rates of RSL rise in the early to mid Holocene (1.0 ± 0.6 m/ka) than in the mid Holocene (0.5 ± 0.5 m/ka). The oldest index point at 6.6 ka places RSL at −4.5 ± 9.0 m. RSL then rose to −2.3 ± 3.8 m at 4.8 ka, -2.0 ± 9.5 m at 3.0 ka, and 0.7 ± 3.0 m at 0.5 ka.

3.20. Suriname and Guyana

Suriname and Guyana's RSL record contains 29 index points from mangrove peat (Roeleveld and van Loon, 1979) (Fig. 8.20). A rise in RSL (8.4 ± 1.1 m/ka) is observed in the early Holocene from −14.4 ± 5.6 m at 9.6 ka (oldest index point) to −4.8 ± 2.7 m at 8.3 ka. RSL continued to rise (4.7 ± 0.8 m/ka) to −1.4 ± 1.8 m at 6.9 ka. The rate of RSL rise slowed (0.8 ± 0.7 m/ka) in the mid to late Holocene, with RSL rising to a highstand of +0.4 ± 1.2 m by 7.2 ka and +0.9 ± 1.0 m at 4.7 ka. RSL fell gradually (−0.1 ± 0.3 m/ka) to present, reaching +0.6 ± 1.4 m by 1.0 ka.

4. Discussion

4.1. Reconstruction of relative sea level in the Caribbean

We build upon previous efforts to produce a Caribbean Holocene RSL database (e.g., Lighty et al., 1982; Toscano and Macintyre, 2003; Milne and Peros, 2013). We add new data for 14 regions in the Caribbean to previous regional compilations by reinterpreting and

expanding on the type of sea-level indicators incorporated in the database. We also correct for effects of local processes (sediment compaction and tidal range change) and use a spatio-temporal statistical model to assess patterns and rates of RSL change through time.

The coral database of Lighty et al. (1982) was developed using *A. palmata* corals sampled from well-documented shallow reef-crest frameworks in the western Caribbean with a living depth range of <1–5 m. Toscano and Macintyre (2003) expanded the Lighty et al. (1982) coral database by adding a regional compilation of mangrove peat that provided an upper constraint on RSL and correcting all ages in the database for isotopic fractionation effects (Stuiver and Polach, 1977). However, they combined all data to produce a single sea-level curve for the region, which precludes examination of spatial variation in RSL due to GIA, tectonics and local scale processes (Toscano et al., 2011). Milne and Peros (2013) updated the database of Toscano and Macintyre (2003) with additional data from Belize, the U.S. Gulf coast, Trinidad, the Yucatan Peninsula of Mexico, and Cuba to compare regional sea-level records with GIA models, although measurement errors of some index points were underestimated (e.g., leveling/elevation errors of Trinidad and Tobago data) and local effects were not examined.

In previous compilations, mangroves (upper limit) and *A. palmata* corals (lower limit) were used to bracket the position of RSL (e.g., Toscano and Macintyre, 2003), or when the indicative meaning of both sample types was considered (e.g., Milne and Peros, 2013), there was no temporal overlap in mangrove and *A. palmata* indicators, and therefore the agreement between assumed depth distributions (indicative meaning) could not be assessed. In our data compilation, numerous sites (Figs. 5.1, 6.6, 6.7, 6.8, 6.9, 7.10, 7.11, 7.12, 7.14) show agreement between mangrove peat, *A. palmata* corals, microbial mats, and beach rock indicators, which provides support for the depth distributions reported for these samples and offers greater confidence in these reconstructions than those based on a single indicator/proxy alone.

4.2. Uncertainty of relative sea-level reconstructions

Sediment compaction is a vertical error that influences mangrove and sedimentary index points and is challenging to quantify (van Asselen et al., 2009). Sediment compaction lowers the altitude of a sea-level index point (A_i) to a depth below where it was initially deposited (e.g., Kaye and Barghoorn, 1964; Allen, 2000). This effect underestimates the value of A_i, which results in RSL estimates that are too low. In temperate marshes this influence has been estimated based on an index point's position in a stratigraphic sequence (Haslett et al., 1998; Edwards, 2006; Shennan et al., 2000b; Shennan and Horton, 2002; Horton and Shennan, 2009; Engelhart and Horton, 2012). We were able to make a first-order assessment of this effect using the stratigraphic position of intercalated samples (0.22 m ± 0.07 m of compaction per meter of overburden) (Fig. 3). Regression on the Jamaica data alone yields 0.3 m compaction per meter overburden, whereas the Central Belize dataset returns a value of 0.1 m compaction per meter overburden. The estimate from Central Belize may be a minimum because it lacks sequences of clastic overburden, which would likely increase compaction (e.g., Allen, 2000). Our estimate of compaction is consistent with those reported for other temperate regions. Horton et al. (2013) found 0.3 m of compaction per meter overburden in New Jersey, USA, and Horton and Shennan (2009) found values ranging from 0.24 to 0.5 m of compaction per meter of overburden on the east coast of England. A compaction study of mangrove sediments from Singapore using geotechnical measurements reported average maximum compaction of 17–55%, which is comparable to values of 13–47% reported for temperate marshes of the US Atlantic and Gulf coast (Bloom, 1964; Kaye and Barghoorn, 1964; Stout and Spackman, 1989; Törnqvist et al., 2008) and England (Haslett et al., 1998). However, Singapore experienced a mid-Holocene sea-level highstand that would result in dewatering of mangrove peats, potentially increasing compaction effects compared to sites that remained waterlogged. Future studies may incorporate geotechnical approaches to more accurately account for sediment compaction at individual sites.

Tidal range change is an additional source of vertical uncertainty that may influence all sea-level indicators (Shennan et al., 2000a; Horton et al., 2013). If tidal range were greater in the past, this would lead to a change in the reference water-level value, and depending on the indicator, RSL estimates could consequently be higher (e.g., corals) or lower (e.g., mangrove peat). Paleotidal range in the Caribbean remained relatively constant throughout the Holocene, with the exception of a large oscillation in the amplitude of tides between 10 and 8 ka, particularly off the western coast of Florida/northern Bahamas and the southern Caribbean coast of Central America (Fig. 4d). The change in tidal amplitude during this time period is consistent with other modeling studies (Arbic et al., 2004; 2008; Uehara et al., 2006), and is related to changes in the area of major dissipation sites, such as the opening/closing of the Hudson Strait, and the natural frequency of the North Atlantic basin nearing resonance frequency around this time (Griffiths and Peltier, 2008, 2009; Hill et al., 2011).

On some coasts, vertical land motion caused by tectonics is an important source of uncertainty in interpreting drivers of Holocene RSL change (e.g., van de Plassche et al., 2014). The Jamaican region lies close to potentially active large reverse faults (DeMets and Wiggins-Grandison, 2007). Although the Jamaican data are consistent with similar latitude regions for most of the Holocene, RSL is anomalously shallow between 8 and 7 ka (Fig. 9). The Dominican region lies near a large transpressional fault and has experienced several major historical earthquakes (Dolan and Wald, 1998), the effect of which on vertical displacement is unknown. The vertical resolution of data (marine limiting dates that have no weight in the spatio-temporal statistical model), however, provides little insight on the impact of this fault system on Dominican RSL. Reef distribution in Belize has been attributed to displacements on recently active normal faults (Lara, 1993; Aronson et al., 2012), but no differential pattern in RSL is discernible among the Belizean sites, suggesting either that these faults are not currently active, the recurrence interval is longer that the Holocene, or vertical displacements are too small to be detectable. Subduction earthquakes could produce substantial vertical displacements at sites located in the Antilles chain; however, the largest known subduction earthquake did not produce substantial displacement on land (Bernard and Lambert, 1988).

Vertical land motion from sedimentary loading of the Orinoco Delta may cause subsidence of the region, which would lower RSL estimates. Warne et al. (1999, 2002) report differential subsidence across the Orinoco Delta, with subsidence rates estimated between 0 and 3.3 m/ka. These estimates are comparable to those from other large river deltas, such as the Mississippi River Delta (Allison et al., 2016). If a highstand did exist, subsidence of that magnitude could offset the effects from ocean syphoning/continental levering, masking evidence of higher than present RSL in the region.

4.3. Regional patterns of relative sea-level change

The Caribbean region represents intermediate- and far-field locations. Early studies of the Caribbean island of Barbados focused on using RSL to directly estimate the eustatic deglacial signal (Fairbanks, 1989), although subsequent investigations

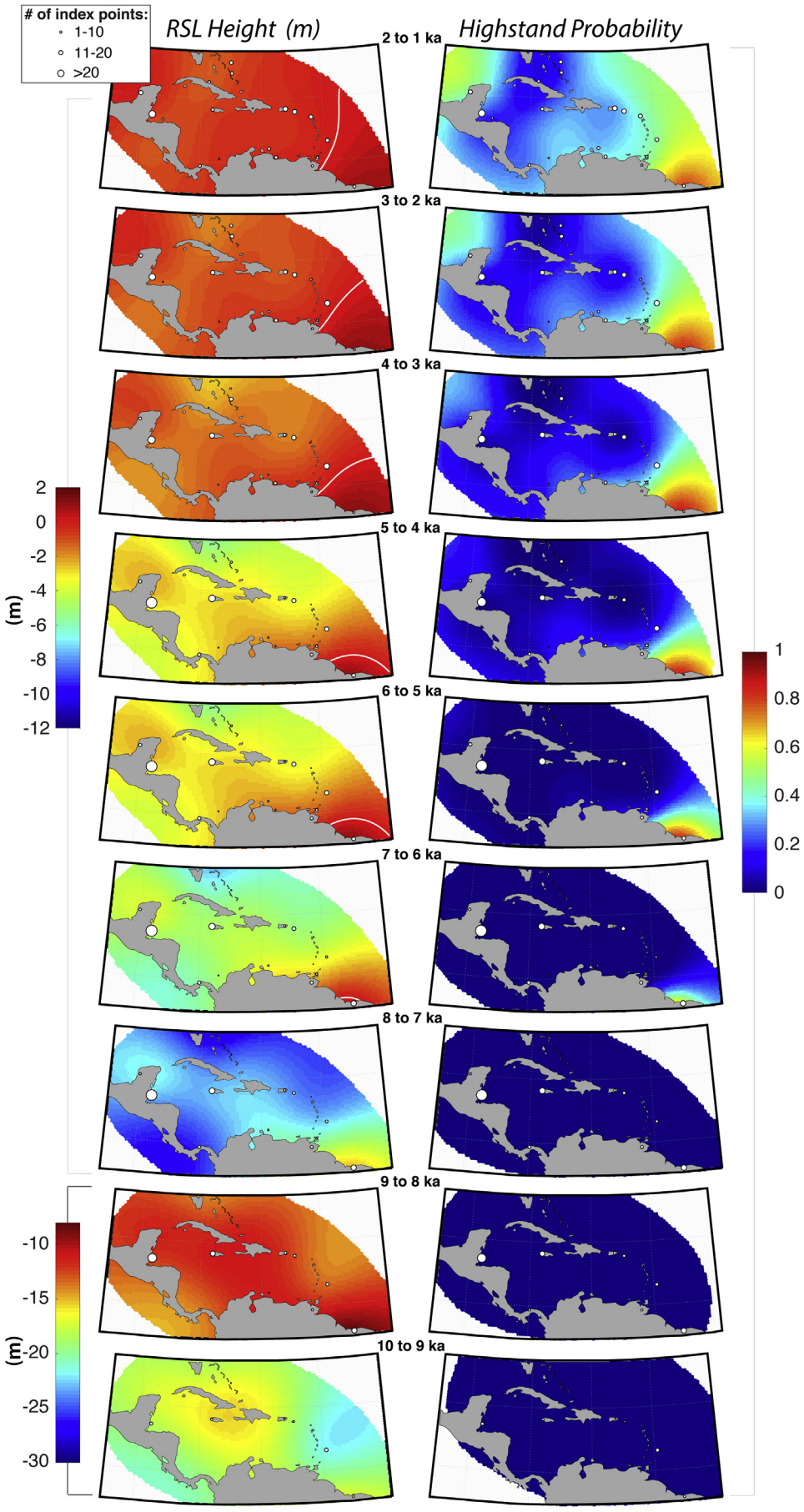

Fig. 9. Mean estimates of rates of RSL change calculated from the spatio-temporal statistical model for (a) each site and (b) over the entire RSL field. Each site is shaded according to its relative distance from the former Laurentide Ice Sheet (a). The size of circles on the maps (b) shows the number of index points within a ±1-ka time window of the time interval shown. Note change in color scale designating rates of RSL change among early (12–8 ka), mid (8–4 ka), and late (4–0 ka) timescales.

indicated that Caribbean RSL has significant influence from GIA-related processes, such as glacio-isostatic subsidence, rotational effects, ocean syphoning, continental levering, and 3-D variations in mantle viscosity structure (Rostami et al., 2000; Lambeck et al., 2002; Milne et al., 2005; Peltier and Fairbanks, 2006; Toscano et al., 2011; Milne and Peros, 2013; Austermann et al., 2013).

To examine temporal variability in RSL records, we calculated 1-ka average rates of change for each site in the database (Fig. 10;

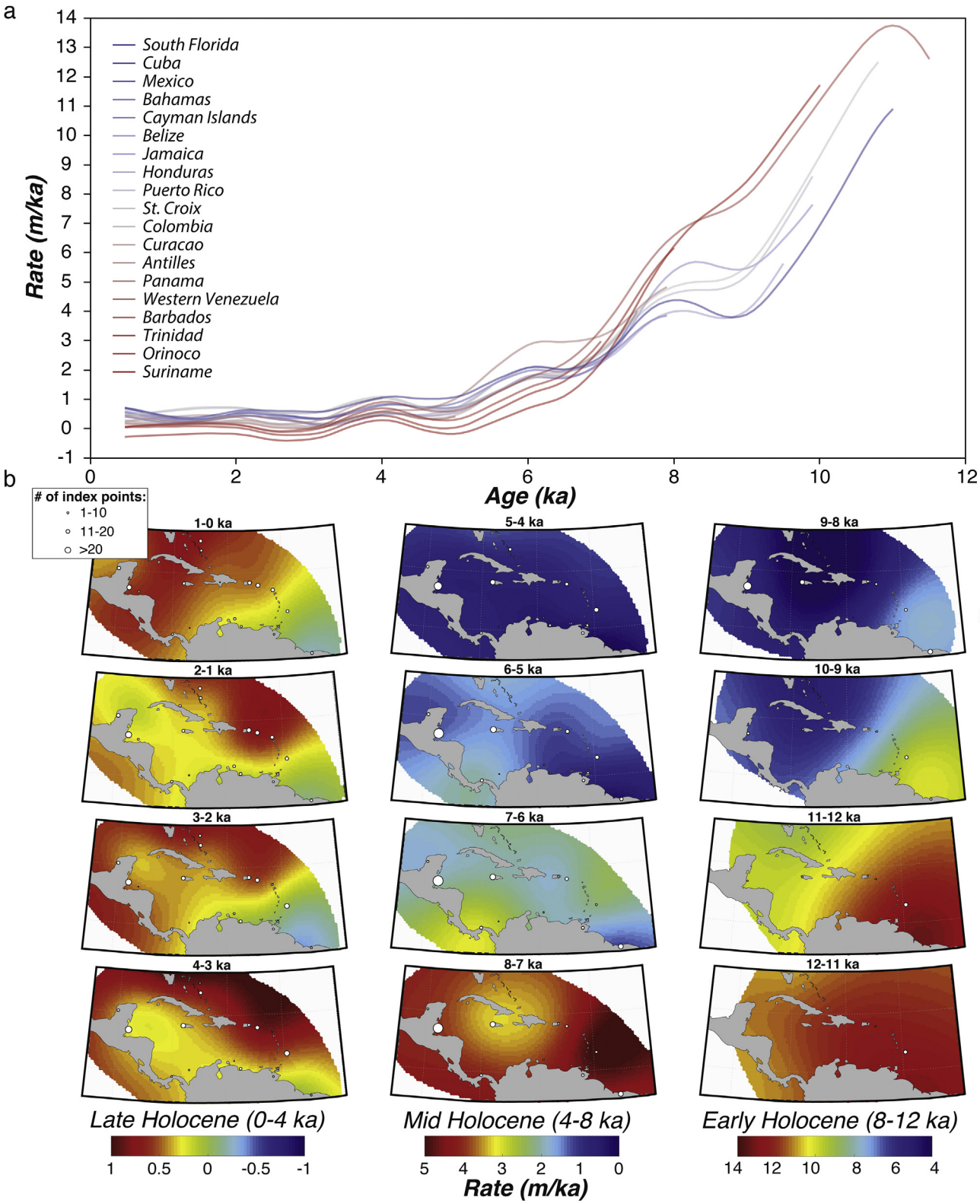

Fig. 10. Maps of Caribbean region estimated from the spatio-temporal statistical model applied to the data showing the height of RSL where 0 is present day level (denoted by white line) and the probability of RSL higher than present level (highstand probability). The size of circles on the maps shows the number of index points within a ± 1-ka time window of the time interval shown. Note change in color scale designating RSL heights between 10–8 ka and 8–0 ka.

Table 4
Average early-, mid-, and late-Holocene rates of RSL change for each site calculated using the empirical hierarchical model.

Site	Average rate (m/ka)		
	4-0 ka	8-4 ka	12-8 ka
South Florida	0.6 ± 0.3	2.1 ± 0.3	7.4 ± 0.7
Cuba	0.5 ± 0.3	1.9 ± 0.3	7.5 ± 0.6
Mexico	0.4 ± 0.3	1.9 ± 0.4	8.4 ± 0.8
Bahamas	0.5 ± 0.3	1.9 ± 0.4	7.6 ± 0.6
Cayman	0.4 ± 0.3	1.8 ± 0.3	7.7 ± 0.7
Belize	0.4 ± 0.2	1.8 ± 0.2	8.3 ± 0.7
Jamaica	0.4 ± 0.2	1.8 ± 0.2	7.8 ± 0.6
Honduras	0.4 ± 0.3	2.0 ± 0.3	8.1 ± 0.7
Dominican Republic	0.4 ± 0.3	1.8 ± 0.4	8.2 ± 0.6
Puerto Rico	0.6 ± 0.3	1.9 ± 0.3	8.8 ± 0.5
St. Croix	0.7 ± 0.3	2.0 ± 0.3	9.0 ± 0.5
Colombia	0.3 ± 0.3	2.0 ± 0.4	8.7 ± 0.6
Curacao	0.2 ± 0.3	1.9 ± 0.4	9.2 ± 0.6
Antilles	0.4 ± 0.3	2.3 ± 0.3	10.1 ± 0.4
Panama	0.4 ± 0.3	2.4 ± 0.4	8.2 ± 0.7
Western Venezuela	0.2 ± 0.3	1.9 ± 0.3	9.4 ± 0.6
Barbados	0.2 ± 0.3	2.3 ± 0.3	10.6 ± 0.4
Trinidad	0.2 ± 0.3	2.0 ± 0.3	10.6 ± 0.4
Orinoco	0.1 ± 0.3	1.7 ± 0.3	10.5 ± 0.5
Suriname and Guyana	−0.2 ± 0.3	1.4 ± 0.3	10.9 ± 0.6

Table 4). The fastest rates of RSL rise are observed in the early Holocene, ranging from 10.9 ± 0.6 m/ka in Suriname and Guyana to 7.4 ± 0.7 m/ka in southern Florida from 12 to 8 ka. Rates began to slow dramatically in the mid Holocene at ~6 to 5 ka. This slowing trend continued in the late Holocene, with rates ranging from 0.6 ± 0.3 m/ka in southern Florida to −0.2 ± 0.3 m/ka in Suriname and Guyana from 4 ka to present. This temporal pattern in rates of RSL change is predominantly driven by the reduction in sea-level equivalent inputs in the early to mid Holocene, coincident with final melting of the LIS at ~7 ka (Peltier, 1998; Carlson et al., 2008; Renssen et al., 2009; Widmann, 2009) and the Scandinavian ice sheet by ~9.5 ka (Karlen, 1979; Carlson and Clark, 2012). Antarctic and Greenland ice input also diminished during this period, although the exact timing and relative contributions from these sources is unresolved (Peltier, 2007; Carlson and Clark, 2012; Lambeck et al., 2014; Peltier, 2015). With the onset of the Holocene Climatic Optimum in high northern latitudes between ~9.5 and 4 ka, there is evidence to suggest that local ice-margin retreat of the Greenland ice sheet (Weidick et al., 1990; Briner et al., 2013; Vasskog et al., 2015) contributed ~ -0.5 to 0.5 m equivalent sea level between ~7 and 5 ka (Tarasov and Peltier, 2002; Simpson et al., 2009; Lecavalier et al., 2014). In contrast, cooling during the Greenland Neoglacial may have caused ice sheet advance responsible for ~0.2 m sea-level equivalent fall (e.g., Lecavalier et al., 2014), but this regrowth overprinted evidence of the ice sheet's mid-Holocene minimum position. Other sources indicate that the Antarctic Thermal Optimum (Hall et al., 2006; Bentley et al., 2009; Verleyen et al., 2011; Anderson et al., 2014) stimulated melt of the western Antarctic ice sheet after ~7 ka (Stone et al., 2003), with melt continuing until 4 ka (Peltier et al., 2015) to 2 ka (Lambeck et al., 2014), although increased ice accumulation rates in the interior of western Antarctica from warmer air temperatures and higher precipitation imply ice mass gains (Siegert and Payne, 2004; Frieler et al., 2015).

The Caribbean RSL data exhibit spatial variability likely driven by a range of processes. To investigate spatial variability of RSL in the region, we used the spatio-temporal statistical model to produce maps of the height of RSL at 1-ka increments from 10 ka to present (Fig. 9, Table 5). To demonstrate uncertainty in the RSL estimates, we show one standard deviation of RSL height (Fig. S1). In the early Holocene (10–8 ka), local highs (in the Greater Antilles chain off the coasts of Jamaica, southeastern Cuba and eastern Haiti) and lows (in the lesser Antilles, Barbados, and Trinidad) in RSL are superimposed over a subtle NNW–SSE oriented gradient with shallower (higher) RSL values occurring with increasing distance from the LIS center. Previous GIA modeling studies from the Caribbean (Milne et al., 2005; Milne and Peros, 2013) show a similar trend and indicate that it results from steady collapse of the proglacial forebulge associated with LIS deglaciation leading to regional land subsidence. Although there is limited spatial coverage of data in the early Holocene, the Caribbean data show increasing rates of RSL rise with greater distance from the LIS (Fig. 10). Milne and Peros (2013) indicate that the gravitational influence of the ice-load changes on sea-surface height drives this RSL gradient. This effect is only active as ice is melting; therefore, the gradient is reduced substantially from 8 ka onwards (when most North American ice had melted), which caused the observed change in RSL rates.

As ice melt slowed in the mid Holocene, spatial variability in the Caribbean appeared in the emergence of a highstand. To examine

Table 5
Heights (±1 standard deviation) of RSL relative to present-day level (0 m) estimated by the empirical hierarchical model.

Site	1 to 0 ka	2 to 1 ka	3 to 2 ka	4 to 3 ka	5 to 4 ka	6 to 5 ka	7 to 6 ka	8 to 7 ka	9 to 8 ka	10 to 9 ka
South Florida	−0.6 ± 0.9	−1.1 ± 0.9	−1.7 ± 0.8	−2.3 ± 0.8	−3.3 ± 0.8	−4.5 ± 0.9	−6.5 ± 0.9	−9.1 ± 0.9	−13.3 ± 1.0	−17.5 ± 1.2
Cuba	−0.8 ± 0.4	−1.3 ± 0.4	−1.8 ± 0.5	−2.2 ± 0.7	−2.9 ± 0.7	−3.9 ± 0.8	−5.9 ± 0.9	−8.3 ± 1.0	−12.2 ± 1.0	−16.3 ± 1.2
Mexico	0.1 ± 0.6	−0.1 ± 0.7	−0.6 ± 0.8	−1.0 ± 0.9	−1.8 ± 1	−2.6 ± 1.1	−4.2 ± 1.2	−6.7 ± 1.3	−12.1 ± 1.5	−18.1 ± 1.8
Bahamas	−1.0 ± 0.4	−1.4 ± 0.5	−1.8 ± 0.7	−2.2 ± 0.8	−3.0 ± 0.9	−4.0 ± 1.1	−5.8 ± 1.2	−8.3 ± 1.2	−12.1 ± 1.3	−16.1 ± 1.4
Cayman	−1.0 ± 0.3	−1.4 ± 0.2	−1.8 ± 0.4	−2.0 ± 0.5	−2.5 ± 0.7	−3.3 ± 0.8	−5.2 ± 0.9	−7.6 ± 0.9	−11.8 ± 1.0	−16.3 ± 1.2
Belize	−0.5 ± 0.4	−0.8 ± 0.4	−1.3 ± 0.4	−1.5 ± 0.4	−2.0 ± 0.3	−2.6 ± 0.3	−4.3 ± 0.3	−6.7 ± 0.3	−11.9 ± 0.6	−17.6 ± 1.1
Jamaica	−0.2 ± 0.4	−0.6 ± 0.3	−0.9 ± 0.3	−1.2 ± 0.3	−1.7 ± 0.3	−2.5 ± 0.3	−4.4 ± 0.3	−6.9 ± 0.3	−10.7 ± 0.6	−15 ± 0.9
Honduras	−0.8 ± 0.4	−1.2 ± 0.4	−1.6 ± 0.5	−1.8 ± 0.6	−2.3 ± 0.7	−3.1 ± 0.8	−5.1 ± 0.8	−7.7 ± 0.8	−12.7 ± 0.9	−18.2 ± 1.2
Dominican Republic	−0.2 ± 1.0	−0.6 ± 1.0	−1.0 ± 1.0	−1.4 ± 1.1	−2.1 ± 1.1	−2.9 ± 1.2	−4.7 ± 1.2	−7.1 ± 1.2	−11.0 ± 1.3	−15.6 ± 1.4
Puerto Rico	0.1 ± 0.8	−0.4 ± 0.8	−1.1 ± 0.8	−1.7 ± 0.9	−2.7 ± 0.9	−3.5 ± 0.9	−5.1 ± 0.9	−7.8 ± 1.0	−12.3 ± 1.1	−17.8 ± 1.2
St. Croix	0.1 ± 0.6	−0.6 ± 0.5	−1.3 ± 0.6	−1.9 ± 0.6	−2.9 ± 0.6	−3.7 ± 0.7	−5.3 ± 0.8	−8.1 ± 0.8	−12.9 ± 1.0	−18.7 ± 1.2
Colombia	−0.2 ± 1.1	−0.4 ± 1.1	−0.7 ± 1.1	−0.8 ± 1.1	−1.3 ± 1.2	−2.1 ± 1.2	−4.1 ± 1.2	−7.0 ± 1.3	−11.5 ± 1.5	−17.0 ± 1.7
Curacao	−0.2 ± 0.9	−0.4 ± 0.9	−0.7 ± 0.9	−0.8 ± 0.9	−1.3 ± 0.9	−1.9 ± 1.0	−3.6 ± 1.0	−6.4 ± 1.1	−11.2 ± 1.3	−17.2 ± 1.6
Antilles	0.4 ± 0.6	0.0 ± 0.6	−0.4 ± 0.7	−0.7 ± 0.8	−1.7 ± 0.8	−2.5 ± 0.9	−4.2 ± 1.0	−7.6 ± 1.0	−13.6 ± 1.1	−21.1 ± 1.1
Panama	−0.5 ± 0.4	−0.8 ± 0.6	−1.2 ± 0.8	−1.5 ± 0.9	−2.1 ± 1.0	−3.2 ± 1.0	−5.9 ± 1.0	−9.2 ± 1.1	−14.0 ± 1.4	−19.4 ± 1.8
Western Venezuela	−0.1 ± 0.5	−0.2 ± 0.4	−0.4 ± 0.3	−0.5 ± 0.3	−1.0 ± 0.4	−1.5 ± 0.6	−3.2 ± 0.8	−6.0 ± 1.0	−11.1 ± 1.3	−17.5 ± 1.6
Barbados	0.5 ± 0.7	0.4 ± 0.7	0.2 ± 0.7	0.1 ± 0.7	−0.7 ± 0.7	−1.4 ± 0.8	−3.1 ± 0.9	−6.6 ± 1.0	−13.1 ± 1.1	−21.2 ± 1.0
Trinidad	0.0 ± 0.7	−0.1 ± 0.8	−0.2 ± 0.8	−0.3 ± 0.8	−0.9 ± 0.8	−1.3 ± 0.8	−2.7 ± 0.9	−5.8 ± 0.9	−12.0 ± 1.1	−20.0 ± 1.2
Orinoco	−0.4 ± 0.5	−0.5 ± 0.4	−0.5 ± 0.5	−0.4 ± 0.4	−0.7 ± 0.4	−0.9 ± 0.4	−2.0 ± 0.5	−4.9 ± 0.8	−10.9 ± 1.1	−18.9 ± 1.3
Suriname and Guyana	0.8 ± 0.6	1.0 ± 0.7	1.2 ± 0.9	1.5 ± 1.0	1.3 ± 0.9	1.3 ± 0.9	0.6 ± 0.8	−1.8 ± 0.8	−7.9 ± 1.0	−16.4 ± 1.5

Table 6
Magnitude and probability of a mid-Holocene highstand in RSL at Suriname and Guyana. RSL Height is given as mean ± 1 s.d. during the 500-year time period listed along with the associated probability of RSL higher than present level (highstand probability).

Time period (ka)	RSL height (m)	Highstand probability
8 to 7.5	−3.35 ± 1.00	0.00
7.5 to 7	−1.21 ± 0.97	0.11
7 to 6.5	−0.07 ± 1.00	0.47
6.5 to 6	0.50 ± 1.03	0.69
6 to 5.5	0.87 ± 1.07	0.79
5.5 to 5	0.98 ± 1.10	0.81
5 to 4.5	0.90 ± 1.10	0.79
4.5 to 5	0.91 ± 1.13	0.79

the spatial extent of the highstand, we used the spatio-temporal statistical model to produce maps showing the probability of RSL higher than present (Fig. 9). The majority of locations in the Caribbean provide no evidence for higher RSL than present. The exception lies along the southern coast of South America. In Suriname and Guyana, RSL exceeded its present level and reached a height of +0.9 ± 1.0 m between 6.7 and 6.6 ka (54% probability of a highstand; Fig. 9, Table 6). At this site, RSL attained a maximum magnitude of +1.1 ± 1.0 m between 5.3 and 5.2 ka (86% probability of a highstand; Fig. 9, Table 6). At this distance away from the LIS, as the magnitude of the eustatic signal diminished, the effects of hydro-isostatic tilting and ocean syphoning outweighed those from forebulge subsidence and rotational feedback and caused RSL to reach a maximum level at this time. These results are consistent with previous modeling studies from the region that estimate the limit of forebulge collapse extends into the Caribbean (Lambeck et al., 2002; Milne et al., 2005; Toscano et al., 2011; Milne and Peros, 2013).

In the late Holocene, the same NNW–SSE oriented gradient in RSL height is observed from forebulge subsidence, although the magnitude of the signal is reduced due to relaxation of GIA (Peltier, 1996). In contrast to the early Holocene when gravitational influence drove patterns of RSL rates, late Holocene (4–0 ka) rates in RSL rise decrease with increasing distance from the LIS center; this trend is related to collapse of the proglacial forebulge of the LIS (Engelhart et al., 2009, 2011). Sites further north are closer to the center of forebulge collapse and therefore exhibit higher rates of late Holocene RSL rise.

Although localized differences in the spatial variability of Caribbean RSL are observed that are not explained by GIA, the magnitude of these variations is small (<1 m), which suggests that cumulated vertical coseismic and interseismic deformation has remained small (<10s of centimeters) at the studied sites over the Holocene compared to other sources of RSL variation. Future GIA modeling studies incorporating 3-D viscosity structure (e.g., Austermann et al., 2013) may help to account for some of these localized variations. Overall, our results are consistent with previous GIA modeling studies from the region that estimate the limit of forebulge collapse (Lambeck et al., 2002; Milne et al., 2005; Toscano et al., 2011; Milne and Peros, 2013), and the improved spatial and temporal coverage of the Caribbean dataset, combined with the spatial statistical modeling approach, offers further support for these observations. Finally, the spatial variability in RSL (Figs. 9 and 10) resulting from GIA and tectonics demonstrates that a single sea-level curve for the region cannot accurately summarize local relative sea-level histories.

5. Conclusions

We produced a database of relative sea-level (RSL) data for the Caribbean region for the past 12 ka from multiple sea-level indicators, including mangrove peat, microbial mats, beach rock and acroporid and massive corals. The database includes 499 sea-level index points and 238 limiting dates, subdivided into 20 regions based on the availability of data, tectonic setting, and distance from the LIS. Most index points (75%) and limiting data (90%) are younger than 8 ka, although there is an atypical temporal distribution with the greatest amount of the data (~26%) occurring between 8 and 6 ka. We expand on previous regional studies by accounting for local RSL factors. We account for sediment compaction using the stratigraphic position (overburden thickness) of index points and incorporate uncertainties due to Holocene tidal range change using a paleotidal model to isolate eustatic, isostatic, and tectonic factors influencing the RSL data.

We apply a spatio-temporal statistical model to the database to make probabilistic assessments of the past position of RSL and estimate its rates of change. We observe the highest rates of RSL change in the early Holocene (maximum of 10.9 ± 0.6 m/ka in Suriname and Guyana; minimum of 7.4 ± 0.7 m/ka in south Florida from 12 to 8 ka). Rates of RSL rise decreased over time in the mid to late Holocene and did not exceed 2.4 ± 0.4 m/ka in any location from 7 ka to present due to reduced input of meltwater. In the majority of locations, RSL did not exceed the present height during the Holocene. The exception lies along the northern coast of South America in Suriname and Guyana, where RSL reached +1.0 ± 1.1 m above present between 5.3 and 5.2 ka (82% probability of RSL higher than present). At such a distance away from the former LIS, the effects from ocean syphoning and continental levering outweigh the influence of subsidence from forebulge collapse. The spatial variability in RSL resulting from GIA and tectonics precludes the use of single sea-level curve to accurately summarize local relative sea-level histories in the region.

Acknowledgements

This research was supported by NSF grants OCE-1458903, OCE-1458904, OCE-1402017, EAR-1419366, CIF21 DIBBs-1443037, 1145200 and ARC-1203415 and the U.S. Geological Survey Coastal and Marine Geology and Climate Research and Development Programs. The authors acknowledge the researchers who collected the original data used in this study and thank them for their assistance, particularly to those who supplied activity ratio measurements for U–Th ages. We also thank our colleagues Matteo Vacchi, Torbjörn Törnqvist, and Marc Hijma for their guidance in aspects of data interpretation. We acknowledge Matt Peros, who shared data with the authors that was helpful in bringing this work into fruition. This paper is a contribution to PALSEA2 and IGCP Project 639. We dedicate this paper to the memory of our colleague Fred Scatena. Any use of trade names herein was for descriptive purposes only and does not imply endorsement by the U.S. Government.

Appendix A. Supplementary data

Supplementary data related to this article can be found at http://dx.doi.org/10.1016/j.quascirev.2016.08.032.

References

Adams, P.N., Opdyke, N.D., Jaeger, J.M., 2010. Isostatic uplift driven by karstification and sea-level oscillation: modeling landscape evolution in north Florida. Geology 38, 531–534. http://dx.doi.org/10.1130/G30592.1.

Adey, W.H., Burke, R., 1976. Holocene bioherms (algal ridges and bank-barrier reefs) of the eastern Caribbean. Geol. Soc. Am. Bull. 87, 95–109. http://dx.doi.org/10.1130/0016-7606(1976)87<95:HBARAB>2.0.CO;2.

Allen, J.R.L., 2000. Holocene coastal lowlands in NW Europe: autocompaction and the uncertain ground. Coast. Estuar. Environ. Sedimentol. Geomorphol. Geoarchaeology 175, 239–252. http://dx.doi.org/10.1144/Gsl.Sp.2000.175.01.18.

Allison, M., Yuill, B., Törnqvist, T., Amelung, F., Dixon, T., Erkens, G., Stuurman, R., Jones, C., Milne, G., Steckler, M., Syvitski, J., Teatini, P., 2016. Global risks and research priorities for coastal subsidence. Eos 97. http://dx.doi.org/10.1029/2016EO055013.

Andersen, C.B., Boardman, M.R., 1988. The depositional evolution of Snow Bay, San Salvador. Proc. Fourth Symp. Geol. Bahamas 7–22.

Anderson, J.B., Conway, H., Bart, P.J., Witus, A.E., Greenwood, S.L., McKay, R.M., Hall, B.L., Ackert, R.P., Licht, K., Jakobsson, M., Stone, J.O., 2014. Ross Sea paleo-ice sheet drainage and deglacial history during and since the LGM. Quat. Sci. Rev., Reconstr. Antarct. Ice Sheet Deglaciation Rais. 100, 31–54. http://dx.doi.org/10.1016/j.quascirev.2013.08.020.

Arbic, B.K., MacAyeal, D.R., Mitrovica, J.X., Milne, G.A., 2004. Ocean tides and Heinrich events. Nature 432, 460. http://dx.doi.org/10.1038/432460a.

Arbic, B.K., Mitrovica, J.X., MacAyeal, D.R., Milne, G.A., 2008. On the factors behind large Labrador Sea tides during the last glacial cycle and the potential implications for Heinrich events. Paleoceanography 23, PA3211. http://dx.doi.org/10.1029/2007PA001573.

Aronson, R.B., Precht, W.F., Macintyre, I.G., Toth, L.T., 2012. Catastrophe and the life span of coral reefs. Ecology 93, 303–313.

Austermann, J., Mitrovica, J.X., Latychev, K., Milne, G.A., 2013. Barbados-based estimate of ice volume at Last Glacial Maximum affected by subducted plate. Nat. Geosci. 6, 553–557. http://dx.doi.org/10.1038/ngeo1859.

Banks, K.W., Riegl, B.M., Shinn, E.A., Piller, W.E., Dodge, R.E., 2007. Geomorphology of the southeast Florida continental reef tract (Miami-Dade, Broward, and palm beach Counties, USA). Coral Reefs 26, 617–633. http://dx.doi.org/10.1007/s00338-007-0231-0.

Bard, E., Arnold, M., Fairbanks, R.G., Hamelin, B., 1993. ^{230}Th-^{234}U and ^{14}C ages obtained by mass spectrometry on corals. Radiocarbon 35, 191–199.

Bard, E., Arnold, M., Hamelin, B., Tisnerat-Laborde, N., Cabioch, G., 1998. Radiocarbon calibration by means of mass spectrometric ^{230}Th/^{234}U and ^{14}C ages of corals: an updated database including samples from Barbados, Mururoa and Tahiti. Radiocarbon 40, 1085–1092.

Bard, E., Hamelin, B., Fairbanks, R.G., 1990. U-Th ages obtained by mass-spectrometry in corals from Barbados - sea-level during the past 130,000 Years. Nature 346, 456–458.

Bentley, M.J., Hodgson, D.A., Smith, J.A., Cofaigh, C.Ó., Domack, E.W., Larter, R.D., Roberts, S.J., Brachfeld, S., Leventer, A., Hjort, C., Hillenbrand, C.-D., Evans, J., 2009. Mechanisms of Holocene palaeoenvironmental change in the Antarctic Peninsula region. Holocene 19, 51–69. http://dx.doi.org/10.1177/0959683608096603.

Benz, H.M., Tarr, A.C., Hayes, G.P., Villaseñor, A., Furlong, K.P., Dart, R.L., Rhea, S., 2010. Seismicity of the Earth 1900–2010 Caribbean Plate and Vicinity (U.S. Geological Survey Open-file Report 2010–1083-A, Scale 1:8,000,000).

Bernard, P., Lambert, J., 1988. Subduction and seismic hazard in the northern Lesser Antilles: Revision of the historical seismicity. Bull. Seismol. Soc. Am. 78, 1965–1983.

Blanchon, P., Jones, B., Ford, D.C., 2002. Discovery of a submerged relic reef and shoreline off Grand Cayman: further support for an early Holocene jump in sea level. Sediment. Geol. 147, 253–270. http://dx.doi.org/10.1016/S0037-0738(01)00143-9.

Blanchon, P., Perry, C.T., 2004. Taphonomic differentiation of *Acropora palmata* facies in cores from Campeche bank reefs, Gulf of México. Sedimentology 51, 53–76. http://dx.doi.org/10.1046/j.1365-3091.2003.00610.x.

Bloom, A.L., 1964. Peat accumulation and compaction in a Connecticut coastal marsh. J. Sediment. Res. 34.

Bradley, S.L., Milne, G.A., Horton, B.P., Zong, Y., 2016. Modelling sea level data from China and Malay-Thailand to estimate Holocene ice-volume equivalent sea level change. Quat. Sci. Rev. 137, 54–68. http://dx.doi.org/10.1016/j.quascirev.2016.02.002.

Brasier, M., Donahue, J., 1985. Barbuda—an emerging reef and lagoon complex on the edge of the Lesser Antilles island are. J. Geol. Soc. 142, 1101–1117. http://dx.doi.org/10.1144/gsjgs.142.6.1101.

Briner, J.P., Håkansson, L., Bennike, O., 2013. The deglaciation and neoglaciation of Upernavik Isstrøm, Greenland. Quat. Res. 80, 459–467. http://dx.doi.org/10.1016/j.yqres.2013.09.008.

Burke, R., Adey, W.H., Macintyre, I.G., 1989. Overview of the Holocene history, architecture and structural components of Tague reef and lagoon. Terr. Mar. Geol. St. Croix U. S. Virgin Isl. Spec. Publ. 8, 105–110.

Carlson, A.E., Clark, P.U., 2012. Ice sheet sources of sea level rise and freshwater discharge during the last deglaciation. Rev. Geophys. 50, RG4007. http://dx.doi.org/10.1029/2011RG000371.

Carlson, A.E., LeGrande, A.N., Oppo, D.W., Came, R.E., Schmidt, G.A., Anslow, F.S., Licciardi, J.M., Obbink, E.A., 2008. Rapid early Holocene deglaciation of the Laurentide ice sheet. Nat. Geosci. 1, 620–624. http://dx.doi.org/10.1038/ngeo285.

Cheng, H., Edwards, R.L., Shen, C.-C., Polyak, V.J., Asmerom, Y., Woodhead, J., Hellstrom, J., Wang, Y., Kong, X., Spötl, C., Wang, X., Calvin Alexander Jr., E., 2013. Improvements in ^{230}Th dating, ^{230}Th and ^{234}U half-life values, and U–Th isotopic measurements by multi-collector inductively coupled plasma mass spectrometry. Earth Planet. Sci. Lett. 371–372, 82–91. http://dx.doi.org/10.1016/j.epsl.2013.04.006.

Cheng, J., Collins, L.S., Holmes, C., 2012. Four thousand years of habitat change in Florida Bay, as indicated by benthic foraminifera. J. Foraminifer. Res. 42, 3–17. http://dx.doi.org/10.2113/gsjfr.42.1.3.

Cohen, K.M., 2003. Differential subsidence within a coastal prism: late-Glacial - Holocene tectonics in the Rhine-Meuse delta, the Netherlands.

Creveling, J.R., Mitrovica, J.X., Hay, C.C., Austermann, J., Kopp, R.E., 2015. Revisiting tectonic corrections applied to Pleistocene sea-level highstands. Quat. Sci. Rev. 111, 72–80. http://dx.doi.org/10.1016/j.quascirev.2015.01.003.

Cuevas, D.N., Sherman, C.E., Ramírez, W., Hubbard, D.K., 2009. Coral growth rates from the Holocene Cañada Honda fossil reef, Southwestern Dominican Republic: comparisons with modern counterparts in high sedimentation settings. Caribb. J. Sci. 45, 94–109. http://dx.doi.org/10.18475/cjos.v45i1.a13.

Davidson, D.D., 2007. Modern Pollen Spectra from Mangrove Ecosystems of the Sabana-Camaguey Archipelago and Ciego de Avila (Unpublished MSc thesis). University of Toronto, Cuba.

Davis, J.H., 1940. The ecology and geologic role of mangroves in Florida. Publ. Carnegie Inst. Wash. 303–412.

Davis, R., Fitzgerald, D., 2003. Beaches and Coasts. Wiley.

Dawes, C.J., 1998. Marine Botany. John Wiley & Sons.

DeMets, C., Jansma, P.E., Mattioli, G.S., Dixon, T.H., Farina, F., Bilham, R., Calais, E., Mann, P., 2000. GPS geodetic constraints on Caribbean-North America plate motion. Geophys. Res. Lett. 27, 437–440.

DeMets, C., Wiggins-Grandison, M., 2007. Deformation of Jamaica and motion of the Gonâve microplate from GPS and seismic data. Geophys. J. Int. 168, 362–378. http://dx.doi.org/10.1111/j.1365-246X.2006.03236.x.

Digerfeldt, G., Hendry, M.D., 1987. An 8000 year Holocene sea-level record from Jamaica: implications for interpretation of Caribbean reef and coastal history. Coral Reefs 5, 165–169. http://dx.doi.org/10.1007/BF00300959.

Dixon, T.H., Farina, F., DeMets, C., Jansma, P., Mann, P., Calais, E., 1998. Relative motion between the Caribbean and North American plates and related boundary zone deformation from a decade of GPS observations. J. Geophys. Res. Solid Earth 103, 15157–15182. http://dx.doi.org/10.1029/97JB03575.

Dolan, J.F., Wald, D.J., 1998. The 1943-1953 north-central Caribbean earthquakes: active tectonic setting, seismic hazards, and implications for Caribbean-North America plate motions. In: Mann, P., Dolan, J.F. (Eds.), Active Strike-slip and Collisional Tectonics of the Northern Caribbean Plate Boundary Zone. Geological Society of America. Special Paper 326.

Ebanks, W.J., 1967. Recent Carbonate Sedimentation and Diagenesis, Amergris Cay. British Honduras (Ph.D. Dissertation). Rice University, Houston, TX.

Edwards, R.J., 2006. Mid- to late-Holocene relative sea-level change in southwest Britain and the influence of sediment compaction. Holocene 16, 575–587. http://dx.doi.org/10.1191/0959683606hl941rp.

Egbert, G.D., Bennett, A.F., Foreman, M.G.G., 1994. TOPEX/POSEIDON Tides Estimated Using a Global Inverse Model.

Engelhart, S.E., Horton, B.P., 2012. Holocene sea level database for the Atlantic coast of the United States. Quat. Sci. Rev. 54, 12–25. http://dx.doi.org/10.1016/j.quascirev.2011.09.013.

Engelhart, S.E., Horton, B.P., Douglas, B.C., Peltier, W.R., Törnqvist, T.E., 2009. Spatial variability of late Holocene and 20th century sea-level rise along the Atlantic coast of the United States. Geology 37, 1115–1118. http://dx.doi.org/10.1130/G30360A.1.

Engelhart, S.E., Peltier, W.R., Horton, B.P., 2011. Holocene relative sea-level changes and glacial isostatic adjustment of the U.S. Atlantic coast. Geology 39, 751–754. http://dx.doi.org/10.1130/G31857.1.

Fairbanks, R.G., 1990. The age and origin of the "Younger Dryas climate event" in Greenland ice cores. Paleoceanography 5, 937–948. http://dx.doi.org/10.1029/PA005i006p00937.

Fairbanks, R.G., 1989. A 17,000-year glacio-eustatic sea level record: influence of glacial melting rates on the Younger Dryas event and deep-ocean circulation. Nature 342, 637–642. http://dx.doi.org/10.1038/342637a0.

Fairbanks, R.G., Mortlock, R.A., Chiu, T.-C., Cao, L., Kaplan, A., Guilderson, T.P., Fairbanks, T.W., Bloom, A.L., Grootes, P.M., Nadeau, M.-J., 2005. Radiocarbon calibration curve spanning 0 to 50,000 years BP based on paired ^{230}Th/^{234}U/^{238}U and ^{14}C dates on pristine corals. Quat. Sci. Rev. 24, 1781–1796. http://dx.doi.org/10.1016/j.quascirev.2005.04.007.

Feller, C., Fournier, M., Imbert, D., Caratini, C., Martin, L., 1990. Datations ^{14}C et palynology d'un sediment tourbex continu (0-7m) dans la mangrove de Guadeloupe (F.WI). Resultats preliminaries. In: Symposium PICG 274/ORSTOM, pp. 193–202. Cayenne.

Frieler, K., Clark, P.U., He, F., Buizert, C., Reese, R., Ligtenberg, S.R.M., van den Broeke, M.R., Winkelmann, R., Levermann, A., 2015. Consistent evidence of increasing Antarctic accumulation with warming. Nat. Clim. Change 5, 348–352. http://dx.doi.org/10.1038/nclimate2574.

Gabriel, J.J., Reinhardt, E.G., Peros, M.C., Davidson, D.E., Hengstum, P.J. van, Beddows, P.A., 2009. Palaeoenvironmental evolution of Cenote Aktun ha (Carwash) on the Yucatan Peninsula, Mexico and its response to Holocene sea-level rise. J. Paleolimnol. 42, 199–213. http://dx.doi.org/10.1007/s10933-008-9271-x. http://link.springer.com/article/10.1007/s10933-008-9271-x.

Gehrels, W.R., Long, A.J., 2007. Quaternary land-ocean interactions: sea-level change, sediments and tsunami. Mar. Geol. 242, 1–4. http://dx.doi.org/10.1016/J.Margeo.2007.05.005.

Gerdes, G., 2010. What are microbial mats? In: Seckbach, J., Oren, A. (Eds.), Microbial Mats, Cellular Origin, Life in Extreme Habitats and Astrobiology. Springer, Netherlands, pp. 3–25.

Gerdes, G., Krumbein, W.E., 1994. Peritidal potential stromatolites — a synopsis. In: Bertrand-Sarfati, J., Monty, C. (Eds.), Phanerozoic Stromatolites II. Springer, Netherlands, pp. 101–129.

Gischler, E., 2003. Holocene lagoonal development in the isolated carbonate platforms off Belize. Sediment. Geol. 159, 113–132. http://dx.doi.org/10.1016/S0037-

0738(03)00098-8.
Gischler, E., Hudson, J.H., 2004. Holocene development of the Belize barrier reef. Sediment. Geol. 164, 223–236. http://dx.doi.org/10.1016/j.sedgeo.2003.10.006.
Gischler, E., Hudson, J.H., 1998. Holocene development of three isolated carbonate platforms, Belize, Central America. Mar. Geol. 144, 333–347. http://dx.doi.org/10.1016/S0025-3227(97)00102-3.
Gladfelter, E.H., Monahan, R.K., Gladfelter, W.B., 1978. Growth rates of five reef-building corals in the northeastern Caribbean. Bull. Mar. Sci. 28, 728–734.
González, C., Urrego, L.E., Martínez, J.I., Polanía, J., Yokoyama, Y., 2010. Mangrove dynamics in the southwestern Caribbean since the "Little Ice Age": a history of human and natural disturbances. Holocene 20, 849–861. http://dx.doi.org/10.1177/0959683610365941.
Goreau, T.F., 1959. The ecology of Jamaican coral reefs I. Species composition and zonation. Ecology 40, 67–90. http://dx.doi.org/10.2307/1929924.
Griffiths, S.D., Hill, D.F., 2015. Tidal modeling. In: Shennan, I., Long, A.J., Horton, B.P. (Eds.), Handbook of Sea-level Research. John Wiley & Sons, Ltd, pp. 438–451.
Griffiths, S.D., Peltier, W.R., 2009. Modeling of polar ocean tides at the last glacial maximum: amplification, sensitivity, and climatological implications. J. Clim. 22, 2905–2924. http://dx.doi.org/10.1175/2008JCLI2540.1.
Griffiths, S.D., Peltier, W.R., 2008. Megatides in the Arctic ocean under glacial conditions. Geophys. Res. Lett. 35, L08605. http://dx.doi.org/10.1029/2008GL033263.
Gutiérrez-Ayala, L.V., Torrescano-Valle, N., Islebe, G.A., 2012. Reconstrucción paleoambiental del Holoceno tardío de la reserva Los Petenes, Península de Yucatán, México. Rev. Mex. Cienc. Geol. 29, 749–763.
Hall, B.L., Hoelzel, A.R., Baroni, C., Denton, G.H., Boeuf, B.J.L., Overturf, B., Töpf, A.L., 2006. Holocene elephant seal distribution implies warmer-than-present climate in the Ross Sea. Proc. Natl. Acad. Sci. 103, 10213–10217. http://dx.doi.org/10.1073/pnas.0604002103.
Hall, G.F., Hill, D.F., Horton, B.P., Engelhart, S.E., Peltier, W.R., 2013. A high-resolution study of tides in the Delaware Bay: past conditions and future scenarios. Geophys. Res. Lett. 40, 338–342. http://dx.doi.org/10.1029/2012GL054675.
Haslett, S.K., Davies, P., Curr, R.H.F., Davies, C.F.C., Kennington, K., King, C.P., Margetts, A.J., 1998. Evaluating late-Holocene relative sea-level change in the Somerset Levels, southwest Britain. Holocene 8, 197–207. http://dx.doi.org/10.1191/095968398669499299.
Hijma, M.P., Engelhart, S.E., Törnqvist, T.E., Horton, B.P., Hu, P., Hill, D.F., 2015. A protocol for a geological sea-level database. In: Shennan, I., Long, A.J., Horton, B.P. (Eds.), Handbook of Sea-level Research. John Wiley & Sons, Ltd, pp. 536–553.
Hill, D.F., Griffiths, S.D., Peltier, W.R., Horton, B.P., Törnqvist, T.E., 2011. High-resolution numerical modeling of tides in the western atlantic, Gulf of Mexico, and Caribbean sea during the Holocene. J. Geophys Res. 116. http://dx.doi.org/10.1029/2010jc006896.
Horton, B.P., Edwards, R.J., Lloyd, J., 2000. Implications of a microfossil-based transfer function in Holocene sea-level studies. In: Shennan, I., Andrews, J.E. (Eds.), Holocene Land-ocean Interaction and Environmental Change Around the North Sea. Geological Society of London, pp. 41–54.
Horton, B.P., Engelhart, S.E., Hill, D.F., Kemp, A.C., Nikitina, D., Miller, K.G., Peltier, W.R., 2013. Influence of tidal-range change and sediment compaction on Holocene relative sea-level change in New Jersey, USA. J. Quat. Sci. 28, 403–411. http://dx.doi.org/10.1002/jqs.2634.
Horton, B.P., Shennan, I., 2009. Compaction of Holocene strata and the implications for relative sealevel change on the east coast of England. Geology 37, 1083–1086. http://dx.doi.org/10.1130/G30042A.1.
Hubbard, D.K., Zankl, H., Heerden, I.V., Gill, I.P., 2005. Holocene reef development along the northeastern St. Croix shelf, Buck island, U.S. Virgin islands. J. Sediment. Res. 75, 97–113. http://dx.doi.org/10.2110/jsr.2005.009.
Hu, P., 2010. Developing a Quality-controlled Postglacial Sea-level Database for Coastal Louisiana to Assess Conflicting Hypotheses of Gulf Coast Sea-level Change (MSc Thesis). Tulane University, New Orleans.
Ignacio Martínez, J., Yokoyama, Y., Gomez, A., Delgado, A., Matsuzaki, H., Rendon, E., 2010. Late Holocene marine terraces of the Cartagena region, southern Caribbean: the product of neotectonism or a former high stand in sea-level? J. South Am. Earth Sci. 29, 214–224. http://dx.doi.org/10.1016/j.jsames.2009.08.010.
Islebe, G., Sánchez, O., 2002. History of late holocene vegetation at Quintana Roo, Caribbean coast of Mexico. Plant Ecol. 160, 187–192. http://dx.doi.org/10.1023/A:1015865932012.
Jaffey, A.H., Flynn, K.F., Glendenin, L.E., Bentley, W.C., Essling, A.M., 1971. Precision measurement of half-lives and specific activities of ^{235}U and ^{238}U. Phys. Rev. C 4, 1889–1906. http://dx.doi.org/10.1103/PhysRevC.4.1889.
Jaramillo, C., Bayona, G., 2000. Mangrove distribution during the holocene in Tribugí Gulf, Colombia. Biotropica 32, 14–22. http://dx.doi.org/10.1111/j.1744-7429.2000.tb00443.x.
Jelgersma, S., 1961. Holocene sea-level changes in The Netherlands. Meded. Geol. Sticht. 7, 1–100.
Jessen, C.A., Pedersen, J.B.T., Bartholdy, J., Seidenkrantz, M.-S., Kuijpers, A., 2008. A late Holocene palaeoenvironmental record from Altona Bay, St. Croix, US Virgin Islands. Geogr. Tidsskr.-Dan. J. Geogr. 108, 59–70. http://dx.doi.org/10.1080/00167223.2008.10649589.
Karlen, W., 1979. Deglaciation dates from northern Swedish Lappland. Geogr. Ann. Ser. Phys. Geogr. 61, 203–210. http://dx.doi.org/10.2307/520913.
Kaye, C.A., Barghoorn, E.S., 1964. Late quaternary sea-level change and crustal rise at Boston, Massachusetts, with notes on the autocompaction of peat. Bull. Geol. Soc. Am. 75, 63–80. http://dx.doi.org/10.1130/0016-7606(1964)75[63:LQSCAC]2.0.CO;2.
Kelsey, H.M., 2015. Geomorphological indicators of past sea levels. In: Shennan, I., Long, A.J., Horton, B.P. (Eds.), Handbook of Sea-level Research. John Wiley & Sons, Ltd, pp. 66–82.
Khan, N.S., 2014. Environmental and Sea-level Reconstruction in Temperate, Subtropical, and Tropical Coastal Wetlands Using Bulk Stable Carbon Isotope Geochemistry and Microfossils (Ph.D. Dissertation). University of Pennsylvania, Philadelphia.
Klosowska, B., 2003. Late Holocene Embayment and Salina Record of Curaçao (Dutch Antilles): Criteria to Monitor Environmental Change and Biodiversity (PhD thesis). Vrije Universiteit, Amsterdam, The Netherlands.
Knowles, J.T., 2008. A 5000-year History of Caribbean Environmental Change and Hurrican Activity Reconstructed from Coast Lake Sediments of the West Indies (Ph.D. Dissertation). Louisiana State University.
Kopp, R.E., Kemp, A.C., Bittermann, K., Horton, B.P., Donnelly, J.P., Gehrels, W.R., Hay, C.C., Mitrovica, J.X., Morrow, E.D., Rahmstorf, S., 2016. Temperature-driven global sea-level variability in the Common Era. Proc. Natl. Acad. Sci. http://dx.doi.org/10.1073/pnas.1517056113, 201517056.
Lambeck, K., Rouby, H., Purcell, A., Sun, Y., Sambridge, M., 2014. Sea level and global ice volumes from the Last Glacial Maximum to the Holocene. Proc. Natl. Acad. Sci. 111, 15296–15303. http://dx.doi.org/10.1073/pnas.1411762111.
Lambeck, K., Yokoyama, Y., Purcell, A., 2002. Into and out of the Last Glacial Maximum: sea-level change during oxygen isotope stages 3 and 2. Quat. Sci. Rev. 21, 343–360.
Lane, C.S., Clark, J.J., Knudsen, A., McFarlin, J., 2013. Late-Holocene paleoenvironmental history of bioluminescent Laguna Grande, Puerto Rico. Palaeogeogr. Palaeoclimatol. Palaeoecol. 369, 99–113. http://dx.doi.org/10.1016/j.palaeo.2012.10.007.
Lara, M.E., 1993. Divergent wrench faulting in the Belize southern lagoon; implications for Tertiary Caribbean plate movements and Quaternary reef distribution. AAPG Bull. 77, 1041–1063.
Lara, R.J., Cohen, M.C.L., 2006. Sediment porewater salinity, inundation frequency and mangrove vegetation height in Bragança, North Brazil: an ecohydrology-based empirical model. Wetl. Ecol. Manag. 14, 349–358. http://dx.doi.org/10.1007/s11273-005-4991-4.
Lecavalier, B.S., Milne, G.A., Simpson, M.J.R., Wake, L., Huybrechts, P., Tarasov, L., Kjeldsen, K.K., Funder, S., Long, A.J., Woodroffe, S., Dyke, A.S., Larsen, N.K., 2014. A model of Greenland ice sheet deglaciation constrained by observations of relative sea level and ice extent. Quat. Sci. Rev. 102, 54–84. http://dx.doi.org/10.1016/j.quascirev.2014.07.018.
Lighty, R.G., Macintyre, I.G., Stuckenrath, R., 1982. *Acropora palmata* reef framework: a reliable indicator of sea level in the western atlantic for the past 10,000 years. Coral Reefs 1, 125–130. http://dx.doi.org/10.1007/BF00301694.
Lighty, R.G., Macintyre, I.G., Stuckenrath, R., 1978. Submerged early Holocene barrier reef south-east Florida shelf. Nature 276, 59–60. http://dx.doi.org/10.1038/276059a0.
Livsey, D., Simms, A.R., 2013. Holocene sea-level change derived from microbial mats. Geology 41, 971–974. http://dx.doi.org/10.1130/G34387.1.
Luettich, R.A., Westerink, J.J., 1991. A solution for the vertical variation of stress, rather than velocity, in a three-dimensional circulation model. Int. J. Numer. Methods Fluids 12, 911–928. http://dx.doi.org/10.1002/fld.1650121002.
Macintyre, I.G., Adey, W.H., 1990. Buck Island Bar, St. Croix, U.S.V.I., A reef that cannot catch up with sea level. Atoll Res. Bull. 336, 1–7. http://dx.doi.org/10.5479/si.00775630.336.1.
Macintyre, I.G., Glynn, P.W., 1976. Evolution of modern Caribbean fringing reef, galeta point, Panama. AAPG Bull. 60, 1054–1072.
Macintyre, I.G., Glynn, P.W., Toscano, M.A., 2007a. The demise of a major *Acropora palmata* bank–barrier reef off the southeast coast of Barbados, West Indies. Coral Reefs 26, 765–773. http://dx.doi.org/10.1007/s00338-007-0259-1.
Macintyre, I.G., Glynn, P.W., Toscano, M.A., 2007b. The destruction of a large *Acropora palmata* bank-barrier reef and subsequent depletion of this reef-building coral off Barbados. W.I. Atoll Res. Bull. 545, 1–29.
Macintyre, I.G., Littler, M.M., Littler, D.S., 1995. Holocene history of Tobacco range, Belize, Central America. Atoll Res. Bull. 430, 1–18.
Macintyre, I.G., Multer, H.G., Zankl, H.L., Hubbard, D.K., Weiss, M.P., Stuckenrath, R., 1985. In: Gabrie, C., Harmelin, M. (Eds.), Growth and Depositional Facies of a Windward Reef Complex (Nonsuch Bay, Antigua, WI), Proceedings of the Fifth International Coral Reef Congress, Tahiti, 27 May-1 June 1985, vol. 6, pp. 605–610. Miscellaneous Paper (B).
Macintyre, I.G., Raymond, B., Stuckenrath, R., 1983. Recent history of a finging reef, Bahia Salina del Sur, Vieques Island, Puerto Rico. Atoll Res. Bull. No. 268, 9.
Macintyre, I.G., Toscano, M.A., Lighty, R.G., Bond, G.B., 2004. Holocene history of the mangrove islands of Twin Cays, Belize, Central America. Atoll Res. Bull. No. 510, 18.
Macintyre, I.G., Toscano, M.A., Lundberg, J., 2008. Complex environmental patterns and Holocene sea-level changes controlling reef histories along northeastern St. Croix, USVI. Atoll Res. Bull. 1–25. http://dx.doi.org/10.5479/si.00775630.556.1.
Mann, P., Taylor, F.W., Burke, K., Kulstad, R., 1984. Subaerially exposed Holocene coral reef, Enriquillo Valley. Dominic. Repub. Geol. Soc. Am. Bull. 95, 1084–1092. http://dx.doi.org/10.1130/0016-7606(1984)95<1084:SEHCRE>2.0.CO;2.
Mauz, B., Ruggieri, G., Spada, G., 2015. Terminal Antarctic melting inferred from a far-field coastal site. Quat. Sci. Rev. 116, 122–132. http://dx.doi.org/10.1016/j.quascirev.2015.03.008.
Mazzullo, S.J., Teal, C.S., Bischoff, W.D., Dimmick-Wells, K., Wilhite, B.W., 2003. Sedimentary architecture and genesis of Holocene shallow-water mud-

mounds, northern Belize. Sedimentology 50, 743–770. http://dx.doi.org/10.1046/j.1365-3091.2003.00575.x.
McCloskey, T.A., Liu, K., 2013. Sedimentary history of mangrove cays in Turneffe islands, Belize: evidence for sudden environmental Reversals. J. Coast. Res. 971–983. http://dx.doi.org/10.2112/JCOASTRES-D-12-00156.1.
McHutchon, A., Rasmussen, C.E., 2011. Gaussian process training with input noise. In: Shawe-Taylor, J., Zemel, R.S., Bartlett, P.L., Pereira, F., Weinberger, K.Q. (Eds.), Advances in Neural Information Processing Systems 24. Curran Associates, Inc, pp. 1341–1349.
McKee, K.L., Cahoon, D.R., Feller, I.C., 2007. Caribbean mangroves adjust to rising sea level through biotic controls on change in soil elevation. Glob. Ecol. Biogeogr. 16, 545–556. http://dx.doi.org/10.1111/j.1466-8238.2007.00317.x.
McLean, R., 2011. Beach rock. In: Hopley, D. (Ed.), Encyclopedia of Modern Coral Reefs, Encyclopedia of Earth Sciences Series. Springer, Netherlands, pp. 107–111.
Mendelssohn, I.A., McKee, K.L., 2000. Salt marshes and mangroves. In: North American Terrestrial Vegetation. Cambridge University Press, Cambridge, pp. 501–536.
Milne, G.A., Gehrels, W.R., Hughes, C.W., Tamisiea, M.E., 2009. Identifying the causes of sea-level change. Nat. Geosci. 2, 471–478. http://dx.doi.org/10.1038/ngeo544.
Milne, G.A., Long, A.J., Bassett, S.E., 2005. Modelling Holocene relative sea-level observations from the Caribbean and South America. Quat. Sci. Rev. 24, 1183–1202. http://dx.doi.org/10.1016/j.quascirev.2004.10.005.
Milne, G.A., Mitrovica, J.X., 1998. Postglacial sea-level change on a rotating Earth. Geophys. J. Int. 133, 1–19. http://dx.doi.org/10.1046/j.1365-246X.1998.1331455.x.
Milne, G.A., Peros, M., 2013. Data–model comparison of Holocene sea-level change in the circum-Caribbean region. Glob. Planet. Change 107, 119–131. http://dx.doi.org/10.1016/j.gloplacha.2013.04.014.
Mitrovica, J.X., Milne, G.A., 2002. On the origin of late Holocene sea-level highstands within equatorial ocean basins. Quat. Sci. Rev. 21, 2179–2190. http://dx.doi.org/10.1016/S0277-3791(02)00080-X.
Mitrovica, J.X., Peltier, W.R., 1991. Free air gravity anomalies associated with glacial isostatic disequilibriu: load history effects on the inference of deep mantle viscosity. Geophys. Res. Lett. 18, 235–238. http://dx.doi.org/10.1029/91gl00208.
Mofjeld, H.O., Venturato, A.J., González, F.I., Titov, V.V., Newman, J.C., 2004. The harmonic constant datum method: options for overcoming datum discontinuities at mixed–diurnal tidal transitions. J. Atmos. Ocean. Technol. 21, 95–104. http://dx.doi.org/10.1175/1520-0426(2004)021<0095:THCDMO>2.0.CO;2.
Monacci, N.M., Meier-Grunhagen, U., Finney, B.P., Behling, H., Wooller, M.J., 2009. Mangrove ecosystem changes during the Holocene at spanish Lookout cay, Belize. Palaeogeogr. Palaeoclimatol. Palaeoecol. 280, 37–46. http://dx.doi.org/10.1016/j.palaeo.2009.05.013.
Muhs, D.R., Pandolfi, J.M., Simmons, K.R., Schumann, R.R., 2012. Sea-level history of past interglacial periods from Uranium-series dating of corals, Curaçao, Leeward Antilles Islands. Quat. Res. 78, 157–169. http://dx.doi.org/10.1016/j.yqres.2012.05.008.
OBIS, 2016. Data from the Ocean Biogeographic Information System. Intergovernmental Oceanographic Commission of UNESCO. Web. http://www.iobis.org.
Peltier, W.R., 2015. The history of Earth's rotation: impacts of deep earth physics and surface climate variability. In: Schubert, G. (Ed.), Treatise on Geophysics, pp. 221–279.
Peltier, W.R., 2007. History of Earth rotation. In: Schubert, G. (Ed.), Treatise Geophys. 243–293.
Peltier, W.R., 2004. Global glacial isostasy and the surface of the ice-age Earth: the ICE-5G (VM2) model and GRACE. Ann. Rev. Earth Planet. Sci. 32, 111–149. http://dx.doi.org/10.1146/annurev.earth.32.082503.144359.
Peltier, W.R., 1998. Postglacial variations in the level of the sea: implications for climate dynamics and solid-Earth geophysics. Rev. Geophys. 36, 603–689. http://dx.doi.org/10.1029/98RG02638.
Peltier, W.R., 1996. Global sea level rise and glacial isostatic adjustment: an analysis of data from the East Coast of North America. Geophys. Res. Lett. 23, 717–720. http://dx.doi.org/10.1029/96GL00848.
Peltier, W.R., Argus, D.F., Drummond, R., 2015. Space geodesy constrains ice age terminal deglaciation: the global ICE-6G_C (VM5a) model. J. Geophys. Res. Solid Earth 120. http://dx.doi.org/10.1002/2014JB011176, 2014JB011176.
Peltier, W.R., Fairbanks, R.G., 2006. Global glacial ice volume and Last Glacial Maximum duration from an extended Barbados sea level record. Quat. Sci. Rev. 25, 3322–3337. http://dx.doi.org/10.1016/j.quascirev.2006.04.010.
Peltier, W.R., Farrell, W.E., Clark, J.A., 1978. Glacial isostasy and relative sea level: a global finite element model. Tectonophysics 50, 81–110. http://dx.doi.org/10.1016/0040-1951(78)90129-4.
Peros, M.C., 2005. Middle to Late Holocene Environmental Change on the North Coast of Cuba (Unpublished dissertation). University of Toronto.
Pirazzoli, P.A., 1991. World Atlas of Holocene Sea-level Changes. Elsevier.
Polach, H.A., 1976. Radiocarbon Dating as a Research Tool in Archaeology - Hopes and Limitations, Symposium on Scientific Methods of Research in the Study of Ancient Chinese Bronzes and South East Asian Metal and Other Archaeological Artifacts. Proc: Australian Natl Univ, Dept Far Eastern History Pub.
Preuss, H., 1979. Progress in Computer Evaluation of Sea Level Data within the IGCP Project No. 61. Presented at the 1978 International Symposium on Coastal Evolution in the Quaternary. Universidade Sao Paulo, Sao Paulo, pp. 104–134.
Ramcharan, E.K., 2005. Late Holocene ecological development of the Graeme Hall swamp, Barbados, west Indies. Caribb. J. Sci. 41, 147–150.
Ramcharan, E.K., McAndrews, J.H., 2006. Holocene development of coastal Wetland at Maracas Bay, Trinidad. West Indies. J. Coast. Res. 581–586. http://dx.doi.org/10.2112/04A-0001.1.
Rasmussen, C.E., Williams, C.K.I., 2006. Gaussian Processes for Machine Learning. The MIT Press. ISBN 0-262-18253-X.
Reimer, P., 2013. IntCal13 and Marine13 radiocarbon age calibration curves 0–50,000 years cal BP. Radiocarbon 55, 1869–1887. http://dx.doi.org/10.2458/azu_js_rc.55.16947.
Renssen, H., Seppä, H., Heiri, O., Roche, D.M., Goosse, H., Fichefet, T., 2009. The spatial and temporal complexity of the Holocene thermal maximum. Nat. Geosci 2, 411–414. http://dx.doi.org/10.1038/ngeo513.
Robbin, D.M., 1984. A new Holocene sea level curve for upper Florida Keys and Florida reef tract. AAPG Bull. 68 http://dx.doi.org/10.1306/AD46113D-16F7-11D7-8645000102C1865D.
Roeleveld, W., van Loon, A.J., 1979. The holocene development of the Young coastal plain of Suriname. Geol. En. Mijnb. 58, 21–28.
Rostami, K., Peltier, W.R., Mangini, A., 2000. Quaternary marine terraces, sea-level changes and uplift history of Patagonia, Argentina: comparisons with predictions of the ICE-4G (VM2) model of the global process of glacial isostatic adjustment. Quat. Sci. Rev. 19, 1495–1525. http://dx.doi.org/10.1016/S0277-3791(00)00075-5.
Rull, V., Vegas-Vilarrúbia, T., de Pernía, N.E., 1999. Palynological record of an early-mid Holocene mangrove in eastern Venezuela. Implications for sea-level rise and disturbance history. J. Coast. Res. 15, 496–504.
Rundle, J.B., 1982. Viscoelastic-gravitational deformation by a rectangular thrust fault in a layered earth. J. Geophys. Res. 87, 7787–7796. http://dx.doi.org/10.1029/JB087iB09p07787.
Schmidt, D.P., 2008. A Palynological and Stratigraphic Analysis of Mangrove Sediments at Punta Galeta, Panama (Ph.D. Dissertation). University of California, Berkeley.
Scholl, D.W., 1964. Recent sedimentary record in mangrove swamps and rise in sea level over the southwestern coast of Florida: Part 2. Mar. Geol. 2, 343–364. http://dx.doi.org/10.1016/0025-3227(64)90047-7.
Scholl, D.W., Stuiver, M., 1967. Recent submergence of southern Florida: a comparison with adjacent coasts and other eustatic data. Geol. Soc. Am. Bull. 78, 437–454. http://dx.doi.org/10.1130/0016-7606(1967)78[437:RSOSFA]2.0.CO;2.
Schubert, C., Valastro, S., Cowart, J.B., 1977. Evidencias de levantamiento reciente de la costa norte-central (Cordillera de La Costa), Venezuella. Acta Científica Venez. 28, 363–372.
Shennan, I., 1989. Holocene crustal movements and sea-level changes in Great Britain. J. Quat. Sci. 4, 77–89. http://dx.doi.org/10.1002/jqs.3390040109.
Shennan, I., 1986. Flandrian sea-level changes in the Fenland. I: the geographical setting and evidence of relative sea-level changes. J. Quat. Sci. 1, 119–153. http://dx.doi.org/10.1002/jqs.3390010204.
Shennan, I., Horton, B., 2002. Holocene land- and sea-level changes in Great Britain. J. Quat. Sci. 17, 511–526. http://dx.doi.org/10.1002/jqs.710.
Shennan, I., Lambeck, K., Flather, R., Horton, B., McArthur, J., Innes, J., Lloyd, J., Rutherford, M., Wingfield, R., 2000a. Modelling western North Sea palaeogeographies and tidal changes during the Holocene. Geol. Soc. Lond. Spec. Publ. 166, 299–319. http://dx.doi.org/10.1144/GSL.SP.2000.166.01.15.
Shennan, I., Lambeck, K., Horton, B., Innes, J., Lloyd, J., McArthur, J., Rutherford, M., 2000b. Holocene isostasy and relative sea-level changes on the east coast of England. Geol. Soc. Lond. Spec. Publ. 166, 275–298. http://dx.doi.org/10.1144/GSL.SP.2000.166.01.14.
Shlemon, R.J., Capacete, J.L., 1976. Application of Holocene geological data for siting coastal nuclear power plants: an example from Puerto Rico. Bull. Int. Assoc. Eng. Geol. – Bull. Assoc. Int. Géologie Ing. 13, 107–111. http://dx.doi.org/10.1007/BF02634769.
Siegert, M.J., Payne, A.J., 2004. Past rates of accumulation in central West Antarctica. Geophys. Res. Lett. 31, L12403. http://dx.doi.org/10.1029/2004GL020290.
Simpson, M.J.R., Milne, G.A., Huybrechts, P., Long, A.J., 2009. Calibrating a glaciological model of the Greenland ice sheet from the Last Glacial Maximum to present-day using field observations of relative sea level and ice extent. Quat. Sci. Rev. 28, 1631–1657. http://dx.doi.org/10.1016/J.Quascirev.2009.03.004.
Smith, T.J., 1992. Forest structure. In: Robertson, A.I., Alongi, D.M. (Eds.), Tropical Mangrove Ecosystems. American Geophysical Union, pp. 101–136.
Stone, J.O., Balco, G.A., Sugden, D.E., Caffee, M.W., Sass, L.C., Cowdery, S.G., Siddoway, C., 2003. Holocene deglaciation of Marie Byrd land, west Antarctica. Science 299, 99–102. http://dx.doi.org/10.1126/science.1077998.
Stout, S.A., Spackman, W., 1989. Notes on the compaction of a Florida peat and the Brandon lignite as deduced from the study of compressed wood. Int. J. Coal Geol. 11, 247–256. http://dx.doi.org/10.1016/0166-5162(89)90117-1.
Stuiver, M., Polach, H.A., 1977. Reporting of ^{14}C data - discussion. Radiocarbon 19, 355–363.
Taggart, B., 1993. Tectonic and eustatic correlations of radiometrically dated marine terraces in northwest Puerto Rico and Isla de Mona, Puerto Rico. University of Puerto Rico, Mayagüez.
Tarasov, L., Peltier, W.R., 2002. Greenland glacial history and local geodynamic consequences. Geophys. J. Int. 150, 198–229.
Taylor, F.W., Mann, P., Valastro, S., Burke, K., 1985. Stratigraphy and radiocarbon Chronology of a subaerially exposed Holocene coral reef, Dominican Republic. J. Geol. 93, 311–332.
Thom, B.G., 1967. Mangrove ecology and deltaic geomorphology: Tabasco, Mexico. J. Ecol. 55, 301–343. http://dx.doi.org/10.2307/2257879.
Tomlinson, P.B., 1986. The Botany of Mangroves. Cambridge University Press.
Törnqvist, T.E., González, J.L., Newsom, L.A., van der Borg, K., de Jong, A.F.M., Kurnik, C.W., 2004. Deciphering Holocene sea-level history on the U.S. Gulf

Coast: a high-resolution record from the Mississippi Delta. Geol. Soc. Am. Bull. 116, 1026. http://dx.doi.org/10.1130/b2525478.1.
Törnqvist, T.E., Rosenheim, B.E., Hu, P., Fernandez, A.B., 2015. Radiocarbon dating and calibration. In: Shennan, I., Long, A.J., Horton, B.P. (Eds.), Handbook of Sea-level Research. John Wiley & Sons, Ltd, pp. 347–360.
Törnqvist, T.E., Wallace, D.J., Storms, J.E.A., Wallinga, J., van Dam, R.L., Blaauw, M., Derksen, M.S., Klerks, C.J.W., Meijneken, C., Snijders, E.M.A., 2008. Mississippi Delta subsidence primarily caused by compaction of Holocene strata. Nat. Geosci. 1, 173–176. http://dx.doi.org/10.1038/ngeo129.
Torrescano, N., Islebe, G.A., 2006. Tropical forest and mangrove history from southeastern Mexico: a 5000 yr pollen record and implications for sea level rise. Veg. Hist. Archaeobotany 15, 191–195. http://dx.doi.org/10.1007/s00334-005-0007-9.
Torrescano-Valle, N., Islebe, G.A., 2012. Mangroves of southeastern Mexico: palaeoecology and conservation. Open Geogr. J. 5, 6–15. http://dx.doi.org/10.2174/1874923201205010006.
Toscano, M.A., Lundberg, J., 1998. Early Holocene sea-level record from submerged fossil reefs on the southeast Florida margin. Geology 26, 255–258. http://dx.doi.org/10.1130/0091-7613(1998)026<0255:EHSLRF>2.3.CO;2.
Toscano, M.A., Macintyre, I.G., 2003. Corrected western Atlantic sea-level curve for the last 11,000 years based on calibrated ^{14}C dates from *Acropora palmata* framework and intertidal mangrove peat. Coral Reefs 22, 257–270. http://dx.doi.org/10.1007/s00338-003-0315-4.
Toscano, M.A., Peltier, W.R., Drummond, R., 2011. ICE-5G and ICE-6G models of postglacial relative sea-level history applied to the Holocene coral reef record of northeastern St Croix, U.S.V.I.: investigating the influence of rotational feedback on GIA processes at tropical latitudes. Quat. Sci. Rev. 30, 3032–3042. http://dx.doi.org/10.1016/j.quascirev.2011.07.018.
Twilley, R.R., Snedaker, A., Yanez-Arancibia, A., Medina, E., 1996. Biodiversity and ecosystem processes in tropical estuaries: perspectives from mangrove ecosystems. In: Mooney, H., Cushman, H., Medina, E. (Eds.), Biodiversity and Ecosystem Functions: a Global Perspective. John Wiley & Sons, New York, pp. 327–370.
Uehara, K., Scourse, J.D., Horsburgh, K.J., Lambeck, K., Purcell, A.P., 2006. Tidal evolution of the northwest European shelf seas from the Last Glacial Maximum to the present. J. Geophys. Res. Oceans 111. http://dx.doi.org/10.1029/2006jc003531.
Urrego, L.E., Correa-Metrio, A., González, C., Castaño, A.R., Yokoyama, Y., 2013. Contrasting responses of two Caribbean mangroves to sea-level rise in the Guajira Peninsula (Colombian Caribbean). Palaeogeogr. Palaeoclimatol. Palaeoecol. 370, 92–102. http://dx.doi.org/10.1016/j.palaeo.2012.11.023.
Valastro, S., Mott Davis, E., Varela, A., 1977. University of Texas at Austin radiocarbon dates XI. Radiocarbon 19, 280–325.
van Asselen, S., Stouthamer, E., van Asch, T.W.J., 2009. Effects of peat compaction on delta evolution: a review on processes, responses, measuring and modeling. Earth Sci. Rev. 92, 35–51. http://dx.doi.org/10.1016/j.earscirev.2008.11.001.
van de Plassche, O., 1995. Evolution of the intra-coastal tidal range in the Rhine-Meuse delta and Flevo Lagoon, 5700-3000 yrs cal B.C. Mar. Geol., Coast. Evol. Quaternary IGCP Proj. 274 (124), 113–128. http://dx.doi.org/10.1016/0025-3227(95)00035-W.
van de Plassche, O., 1986. Sea-level Research: A Manual for the Collection and Evaluation of Data. Geobooks, Norwich.
van de Plassche, O., 1982. Sea-level change and water-level movements in the Netherlands during the Holocene. Meded. Rijks Geol. Dienst 36, 1–93.
van de Plassche, O., Wright, A.J., Horton, B.P., Engelhart, S.E., Kemp, A.C., Mallinson, D., Kopp, R.E., 2014. Estimating tectonic uplift of the Cape Fear Arch (south-eastern United States) using reconstructions of Holocene relative sea level. J. Quat. Sci. 29, 749–759. http://dx.doi.org/10.1002/jqs.2746.
van Dijk, G.J., Berendsen, H.J.A., Roeleveld, W., 1991. Holocene water level development in the Netherlands' river area; implications for sea-level reconstruction. Geol. En. Mijnb. 70, 311–326.
Vane, C.H., Kim, A.W., Moss-Hayes, V., Snape, C.E., Diaz, M.C., Khan, N.S., Engelhart, S.E., Horton, B.P., 2013. Degradation of mangrove tissues by arboreal termites (*Nasutitermes acajutlae*) and their role in the mangrove C cycle (Puerto Rico): Chemical characterization and organic matter provenance using bulk δ^{13}C, C/N, alkaline CuO oxidation-GC/MS, and solid-state ^{13}C NMR. Geochem. Geophys. Geosystems 14, 3176–3191. http://dx.doi.org/10.1002/ggge.20194.
Vasskog, K., Langebroek, P.M., Andrews, J.T., Nilsen, J.E.Ø., Nesje, A., 2015. The Greenland Ice Sheet during the last glacial cycle: current ice loss and contribution to sea-level rise from a palaeoclimatic perspective. Earth Sci. Rev. 150, 45–67. http://dx.doi.org/10.1016/j.earscirev.2015.07.006.
Velez, M.I., Escobar, J., Brenner, M., Rangel, O., Betancourt, A., Jaramillo, A.J., Curtis, J.H., Moreno, J.L., 2014. Middle to late Holocene relative sea level rise, climate variability and environmental change along the Colombian Caribbean coast. Holocene. http://dx.doi.org/10.1177/0959683614534740, 0959683614534740.
Verleyen, E., Hodgson, D.A., Sabbe, K., Cremer, H., Emslie, S.D., Gibson, J., Hall, B., Imura, S., Kudoh, S., Marshall, G.J., McMinn, A., Melles, M., Newman, L., Roberts, D., Roberts, S.J., Singh, S.M., Sterken, M., Tavernier, I., Verkulich, S., de Vyver, E.V., Van Nieuwenhuyze, W., Wagner, B., Vyverman, W., 2011. Post-glacial regional climate variability along the East Antarctic coastal margin—Evidence from shallow marine and coastal terrestrial records. Earth Sci. Rev. 104, 199–212. http://dx.doi.org/10.1016/j.earscirev.2010.10.006.
Vezina, J., Jones, B., Ford, D., 1999. Sea-level highstands over the last 500,000 years; evidence from the Ironshore formation on Grand Cayman, British West Indies. J. Sediment. Res. 69, 317–327. http://dx.doi.org/10.2110/jsr.69.317.
Warne, A.G., Aslan, A., White, W.A., Gibeaut, J.C., Tremblay, T.A., Smyth, R.C., Guevara, E.H., Gutierrez, R., Hovorka, S.D., Raney, J.A., 1999. Final Report Year Two: Geoenvironmental characterization of the Delta del Orinoco: Report to Petróleos de Venezuela. The University of Texas at Austin Bureau of Economic Geology, 327 pp.
Warne, A.G., Guevara, E.H., Aslan, A., 2002. Late Quaternary evolution of the Orinoco delta, Venezuela. J. Coast. Res. 18, 29.
Weber, J.C., Dixon, T.H., DeMets, C., Ambeh, W.B., Jansma, P., Mattioli, G., Saleh, J., Sella, G., Bilham, R., Pérez, O., 2001. GPS estimate of relative motion between the Caribbean and South American plates, and geologic implications for Trinidad and Venezuela. Geology 29, 75–78. http://dx.doi.org/10.1130/0091-7613(2001)029<0075:GEORMB>2.0.CO;2.
Weidick, A., Oerter, H., Reeh, N., Thomsen, H.H., Thorning, L., 1990. The recession of the inland ice margin during the Holocene climatic optimum in the Jakobshavn Isfjord area of West Greenland. Palaeogeogr. Palaeoclimatol. Palaeoecol. 82, 389–399.
Weiss, M.P., 1979. A saline lagoon on Cayo Sal, western Venezuela. Atoll Res. Bull. No. 232, 1–34.
Widmann, M., 2009. Palaeoclimate: delayed Holocene warming. Nat. Geosci. 2, 380–381. http://dx.doi.org/10.1038/ngeo536.
Woodroffe, C.D., 1983. Development of mangrove swamps behind beach ridges, Grand Cayman Island. West indies. Bull. Mar. Sci. 33, 864–880.
Woodroffe, S.A., 2006. Holocene Relative Sea-level Changes in Cleveland Bay, North Queensland, Australia (PhD thesis). Durham University, Durham, UK.
Wooller, M.J., Behling, H., Guerrero, J.L., Jantz, N., Zweigert, M.E., 2009. Late Holocene hydrologic and vegetation changes at Turneffe Atoll, Belize, compared with records from mainland central America and Mexico. Palaios 24, 650–656. http://dx.doi.org/10.2110/palo.2009.p09-036r.
Wooller, M.J., Morgan, R., Fowell, S., Behling, H., Fogel, M., 2007. A multiproxy peat record of Holocene mangrove palaeoecology from Twin Cays, Belize. Holocene 17, 1129–1139. http://dx.doi.org/10.1177/0959683607082553.
Wooller, M., Smallwood, B., Scharler, U., Jacobson, M., Fogel, M., 2003. A taphonomic study of δ^{13}C and δ^{15}N values in *Rhizophora mangle* leaves for a multi-proxy approach to mangrove palaeoecology. Org. Geochem 34, 1259–1275. http://dx.doi.org/10.1016/s0146-6380(03)00116-5.
Yu, T.-T., Rundle, J.B., Fernandez, J., 1996. Surface deformation due to a strike-slip fault in an inelastic gravitational layer overlying a viscoelastic gravitational half-space. J. Geophys. Res. 101, (B2), 3199–3214. http://dx.doi.org/10.1029/95JB03118.